Electronic Supplementary Material (ESI) for Journal of Materials Chemistry A.

Supporting Information

Building-up Interrelationship between Isomeric Benzyl Inner Side Chains within Nonfullerene Acceptor and Isomeric Xylene Solvents for Non-Chlorinated Solvent-Processed Organic Solar Cells

Seonghun Jeong,[a,†] Jeewon Park,[a,†] Yutong Ji,[c,†] Yongjoon Cho,[a,d] Byongkyu Lee,[a,e] Mingyu Jeong,[a,f] Sungwoo Jung,[a] Sangjin Yang,[a] Youdi Zhang,[c]* Seong-Jun Yoon,[a]* and Changduk Yang[a,b]*

[a]School of Energy and Chemical Engineering, Perovtronics Research Center, Low Dimensional Carbon Materials Center, Ulsan National Institute of Science and Technology (UNIST), 50 UNIST-gil, Ulju-gun, Ulsan 44919, South Korea.

[b]Graduate School of Carbon Neutrality, Ulsan National Institute of Science and Technology (UNIST), 50 UNIST-gil, Ulju-gun, Ulsan 44919, South Korea.

[c]College of Chemistry, Key Laboratory of Advanced Green Functional Materials, Changchun Normal University, Changchun 130032, China

[d]Department of Chemistry and Materials Research Center, Northwestern University, 2145 Sheridan Road, Evanston, IL 60208, USA.

[e]Department of Physics and Organic and Carbon Electronics Laboratories (ORaCEL), North Carolina State University, Raleigh, NC 27695, USA

[f]KEPCO Research Institute, Korea Electric Power Corporation, 105, Munji-ro, Yuseong-gu, Daejeon 34056, Republic of Korea.

E-mail: yang@unist.ac.kr, yoonsj@unist.ac.kr, zhangyd@ccsfu.edu.cn

[†]These authors contributed equally to this work.

Materials and Characteristics: 4,7-Dibromo-5,6-dinitrobenzo[c][1,2,5]thiadiazole and trimethyl(6-undecylthieno[3,2-b]thiophen-2-yl)stannane were synthesized according to previously reported methods. 1,2-bis(bromomethyl)benzene, 1,3-bis(bromomethyl)benzene, and 1,4-bis(bromomethyl)benzene were purchased from combi-blocks. The other chemicals and reagents were purchased from Sigma-Aldrich, Tokyo Chemical Industry Co., Ltd, and Alfa Aesar Chemical Company and used without any further purification. All solvents are ACS and anhydrous grade by distillation. 1D ^{1}H NMR and ^{13}C NMR spectra of the intermediates and target products were recorded on a Bruker AVANCE III HD 400 MHz and Varian VNMRS 600 600 MHz spectrometer using deuterated $CDCl_3$, *o*-xylene-d$_{10}$, *m*-xylene-d$_{10}$, and *p*-xylene-d$_{10}$ as solvent and tetramethylsilane (TMS) as an internal standard. (**Fig. 5** and **Fig. S18-S33**). DOSY mode 2D-NMR spectra of the *o*-BzY, *m*-BzY, and *p*-BzY were measured on Varian VNMRS 600 600 MHz. For measuring UV-vis spectra of the *o*-BzY, *m*-BzY, and *p*-BzY, their solutions (4.00 mg mL^{-1} in *o*-xylene, *m*-xylene, and *p*-xylene) were used and the films were prepared by deposition from the 4.00 mg mL^{-1} concentrated xylenes solution *via* the spin-casting method at 700 rpm. The optical bandgaps were estimated from the absorption onset of the as-cast thin films. CV measurements were performed on an Iviumstat.h with a three-electrode cell system in a nitrogen bubbled 0.1 M tetra-*n*-butylammonium hexafluorophosphate (*n*-Bu_4NPF_6) solution in acetonitrile at a scan rate of 100 mV^{-1} s^{-1} at room temperature. An Ag/Ag$^+$ electrode, platinum wire, and material-coated glassy carbon electrode were used as the reference electrode, counter electrode, and working electrode, respectively. The Ag/Ag$^+$ reference electrode was calibrated using a Fc/Fc$^+$ redox couple as an internal standard, whose oxidation potential was set at −4.8 eV with respect to the zero-vacuum level. HOMO and LUMO energy levels of NFAs were obtained from the equation HOMO (eV) $= -(E_{ox}^{onset} - E_{Fc}^{onset} + 4.8)$ and LUMO (eV) $= -(E_{red}^{onset} - E_{Fc}^{onset} + 4.8)$. The ultraviolet photoelectron spectroscopy (UPS) analysis chamber was equipped with a hemispherical electron-energy analyzer (Kratos Ultra Spectrometer) and was maintained at 1.0×10^{-9} Torr. The TGA curves were evaluated with a Q500 (TA Instruments) with a scan rate of 5 °C min^{-1}. The contact angles of BzY-series NFAs and PM6 were obtained using the Phoenix 300 Model instrument.

AFM images of active layer film were recorded using Dimension ICON microscope (Bruker Nano Surface) running with a Nano scope V controller. Grazing incidence wide-angle X-ray scattering (GIWAXS) measurement was conducted at the PLS-II 6D beamline of the Pohang Accelerator Laboratory in Korea. The X-rays coming from the in-vacuum undulator were monochromated ($\lambda = 1.10994$ Å) using a double crystal monochromator and focused both horizontally and vertically (450 (H) × 60 (V) μm^2 in FWHM (full width at half maximum) @sample position) using K–B type mirrors. The GIWAXS sample stage was equipped with a 7-axis motorized stage for the fine alignment of the sample, and the incidence angle of the X-ray beam was set to be 0.12° for the neat and blend films. The GIWAXS patterns were recorded with a 2D CCD detector (Rayonix SX165) and the X-ray irradiation time was 5–30 s, dependent on the saturation level of the detector. Diffraction angles were calibrated using a sucrose standard (monoclinic, P21, a = 10.8631 Å, b = 8.7044 Å, c = 7.7624 Å, and β = 102.938°) and the sample-to-detector distance was ≈231 mm. CCL was calculated according to the following Scherrer equation:

$$CCL = \frac{2\pi K}{\Delta_q}$$

In this equation, CCL is the crystal coherence length, K is a shape factor (0.9), and Δ_q is the FWHM of a diffraction peak.

Device fabrication: The PSCs were fabricated with a configuration of ITO/PEDOT:PSS/active layer/PDINO/Al, where ITO, PEDOT:PSS, and PDINO refer to indium tin oxide, poly(3,4-ethylenedioxythiophene):poly(styrene sulfonate), and perylene diimide functionalized with amino N-oxide, respectively. The ITO-coated glass substrates were rinsed using ultrasonic treatment in deionized water, acetone, and isopropyl alcohol for 20 min and were subsequently dried overnight in oven. the ITO glass substrates were treated with ultraviolet-ozone plasma to eliminate any remaining organic components. PEDOT:PSS aqueous solution (Bayer Baytron AI 4083) was spin-coated at 4000rpm onto the ITO surface, followed by annealing at 150 °C for 20min in ambient atmosphere. Then, they were transferred into a glove box filled with inert nitrogen gas. For the bulk heterojunction based solar cells, active layers were spun onto the PEDOT:PSS layer at 2000 rpm for 40 s from PM6:NFA hot xylene solution (80 °C) in the absence of any additive. Without thermal annealing treatment, methanol solution of PDINO with a concentration of 1.0 mg mL^{-1} was spin-coated onto the as-cast active layer at 3000 rpm for 30 s. Finally, the 100 nm aluminum was deposited under vacuum ($< 3.0 \times 10^{-6}$ Pa). The active area of each sample was 0.042 cm^2.

Solar cell characterization: The current density versus voltage (*J-V*) characteristics were measured using a Keithley 2400 source under AM 1.5G solar illumination with an intensity of 100 mW cm^{-2}. The EQE measurement was conducted by Solar Cell Spectral Response Measurement System QE-R3011 (EnliTech.) in ambient condition.

Morphology characterization: The samples were prepared by spin-coating on the glass substrate for AFM. AFM images of active layer film were recorded using Dimension ICON microscope (Bruker Nano Surface) running with a Nano scope V controller.

Material synthesis:

1-(bromomethyl)-2-hexylbenzene (1a)

To a magnesium tuning in tetrahydrofuran (800 mL), 1-bromopentane (4.7 mL, 37.9 mmol) was added dropwise and gently reflux for 2 h under argon protection. After cooling to room temperature, the mixture was transferred dropwise *via* syringe into a two-neck flask containing a solution of 1,2-bis(bromomethyl)benzene (4 g, 15.2 mmol) and copper(I) bromide methyl sulfide complex (1.28 g, 53.0 mmol) in 800 mL of tetrahydrofuran (THF) at 0 °C. The temperature was kept for 4 h with vigorous stirring. The mixture was quenched with water and the organic layer was extracted by dichloromethane (DCM), dried over magnesium sulfate. The residue was purified with column chromatography with hexane as an eluent to afford the colorless liquid (1.47 g, 38%). ^{1}H NMR ($CDCl_3$, 400 MHz), δ (ppm): 7.33 (dd, $J = 7.5$, 1.4 Hz, 1H), 7.28 − 7.22 (m, 1H), 7.18 (m, 2H), 4.55 (s, 2H), 2.82 − 2.62 (m, 2H), 1.65 (m, 2H), 1.48 − 1.26 (m, 6H), 1.00 − 0.65 (m, 3H).

1-(bromomethyl)-3-hexylbenzene (1b)

The starting material was 1,3-bis(bromomethyl)benzene, (45%, 1.74 g). ^{1}H NMR ($CDCl_3$, 400 MHz), δ (ppm): 7.28 − 7.25 (m, 1H), 7.21 (m, 2H), 7.11 (m, 1H), 4.49 (s, 2H), 1.61 (m, 2H), 1.41 − 1.26 (m, 6H), 0.97 − 0.78 (m, 3H).

1-(bromomethyl)-4-hexylbenzene (1c)

The starting material was 1,4-bis(bromomethyl)benzene, (43%, 1.66 g). ^{1}H NMR ($CDCl_3$, 400 MHz), δ (ppm): 7.30 (m, 2H), 7.15 (m, 2H), 4.50 (s, 2H), 2.59 (m, 2H), 1.60 (m, 2H), 1.42 − 1.19 (m, 6H), 0.95 − 0.82 (m, 3H).

5,6-dinitro-4,7-bis(6-undecylthieno[3,2-*b*]thiophen-2-yl)benzo[*c*][1,2,5]thiadiazole (2)

In a two-neck round-bottom flask, 4,7-dibromo-5,6-dinitrobenzo[c][1,2,5]thiadiazole (3 g, 7.81 mmol), trimethyl(6-undecylthieno[3,2-b]thiophen-2-yl)stannane (8.22 g, 17.97 mmol), and tetrakis(triphenylphosphine)palladium(0) (0.45 g, 0.39 mmol) were dissolved in 30 mL of anhydrous toluene under argon atmosphere. The mixture was stirred and refluxed overnight. After cooling to room temperature, the solvent was evaporated under reduced pressure. The residue was purified by column chromatography using hexane and dichloromethane as an eluent to afford the red solid (5.63 g, 89%). ^{1}H NMR (400 MHz, $CDCl_3$), δ (ppm): 7.71 (s, 2H), 7.18 (s, 2H), 2.77 (m, 4H), 1.79 (m, 4H), 1.46 – 1.15 (m, 32H), 0.94 – 0.80 (m, 6H).

12,13-bis(2-hexylbenzyl)-3,9-diundecyl-12,13-dihydro-[1,2,5]thiadiazolo[3,4-*e*]thieno[2″,3″:4′,5′]thieno[2′,3′:4,5]pyrrolo[3,2-*g*]thieno[2′,3′:4,5]thieno[3,2-*b*]indole (3a)

Compound **2** (0.9 g, 1.11 mmol) and triethyl phosphite (14 mL) were dissolved in anhydrous *o*-dichlorobenzene (14 mL) under argon atmosphere. The mixture was stirred and heated at 180 °C for 10 hours. After cooling to room temperature, the reaction mixture was extracted with brine and dichloromethane and dried over magnesium sulfate. After concentrating the reaction mixture under reduced pressure, the residue was transferred to two-neck round-bottom flask. Subsequently, potassium carbonate (922 mg, 6.66 mmol), potassium iodide (1.10 g, 6.66

mmol), and dimethylformamide (15 mL) were added into the flask and refluxed at 80 °C for an hour under argon atmosphere. Then, compound **1a** (1.42 g, 5.55 mmol) was added and stirred at 130 °C overnight. After cooling to room temperature, the reaction mixture was extracted with DI water and dichloromethane, dried over magnesium sulfate. The residue was purified by column chromatography with hexane and dichloromethane as an eluent to obtain the yellow solid (486.3 mg, 40%). ^{1}H NMR (400 MHz, $CDCl_3$), δ (ppm): 7.49 (d, *J* = 7.6 Hz, 2H), 7.36 – 7.30 (m, 2H), 7.24 – 7.16 (m, 4H), 6.75 (s, 2H), 5.39 (s, 4H), 2.71 (t, *J* = 7.7 Hz, 4H), 1.77 (m, 4H), 1.66 – 1.59 (m, 4H), 1.38 – 1.20 (m, 44H), 0.92 – 0.83 (m, 12H).

12,13-bis(3-hexylbenzyl)-3,9-diundecyl-12,13-dihydro-[1,2,5]thiadiazolo[3,4-*e*]thieno[2′′,3′′:4′,5′]thieno[2′,3′:4,5]pyrrolo[3,2-*g*]thieno[2′,3′:4,5]thieno[3,2-*b*]indole (3b)

Compound **1a** was replaced with compound **1b** (498.5 mg, 41%). ^{1}H NMR (400 MHz, $CDCl_3$), δ (ppm): 7.31 (t, *J* = 7.5 Hz, 2H), 7.24 (d, *J* = 7.5 Hz, 2H), 7.00 – 6.95 (m, 4H), 6.88 (d, *J* = 1.0 Hz, 2H), 5.56 (s, 4H), 2.83 (t, *J* = 7.7 Hz, 4H), 2.66 – 2.58 (m, 4H), 1.88 (m, 4H), 1.63 – 1.56 (m, 4H), 1.34 (d, *J* = 7.9 Hz, 40H), 0.99 – 0.90 (m, 12H).

12,13-bis(4-hexylbenzyl)-3,9-diundecyl-12,13-dihydro-[1,2,5]thiadiazolo[3,4-*e*]thieno[2′′,3′′:4′,5′]thieno[2′,3′:4,5]pyrrolo[3,2-*g*]thieno[2′,3′:4,5]thieno[3,2-*b*]indole (3c)

Compound **1a** was replaced with compound **1c** (547.1 mg, 45%). ^{1}H NMR (400 MHz, $CDCl_3$), δ (ppm): 7.20 (d, *J* = 7.9 Hz, 4H), 7.05 (d, *J* = 7.9 Hz, 4H), 6.88 (s, 2H), 5.54 (s, 4H), 2.83 (t, *J* = 7.7 Hz, 4H), 2.72 (t, *J* = 7.7 Hz, 4H), 1.88 (m, 4H), 1.72 (m, 4H), 1.52 – 1.30 (m, 40H), 1.02 – 0.93 (m, 12H).

12,13-bis(2-hexylbenzyl)-3,9-diundecyl-12,13-dihydro-[1,2,5]thiadiazolo[3,4-e]thieno[2'',3'':4',5']thieno[2',3':4,5]pyrrolo[3,2-g]thieno[2',3':4,5]thieno[3,2-b]indole-2,10-dicarbaldehyde (4a)

Anhydrous dimethylformamide (0.7 m L), phosphorus oxychloride (0.7 mL) and 1,2-dichloroethane (2 mL) were mixed at 0 °C in a two-neck round-bottom flask and the mixture was stirred for an hour. Then, the mixture was transferred dropwise to the solution of compound **3a** (486 mg, 0.44 mmol) in 1,2-dichloroethane (7 mL) and stirred at 130 °C overnight. The reaction mixture was quenched with sodium hydrogen carbonate over three hours, extracted with dichloromethane, and dried over magnesium sulfate. The residue was purified by column chromatography with hexane and dichloromethane as an eluent to afford the orange solid (0.46 g, 91%). ^{1}H NMR (400 MHz, $CDCl_3$), δ (ppm): 9.94 (s, 2H), 7.37 (m, 4H), 7.23 (m, 4H), 5.40 (s, 4H), 3.03 (t, *J* = 7.7 Hz, 4H), 1.82 (m, 4H), 1.67 – 1.59 (m, 4H), 1.36 – 1.20 (m, 44H), 0.89 (m, 12H).

12,13-bis(3-hexylbenzyl)-3,9-diundecyl-12,13-dihydro-[1,2,5]thiadiazolo[3,4-e]thieno[2'',3'':4',5']thieno[2',3':4,5]pyrrolo[3,2-g]thieno[2',3':4,5]thieno[3,2-b]indole-2,10-dicarbaldehyde (4b)

Compound **3a** was replaced with compound **3b** (459.8 mg, 90%). ^{1}H NMR (400 MHz, $CDCl_3$), δ (ppm): 10.06 (s, 2H), 7.33 (t, *J* = 7.5 Hz, 2H), 7.27 (d, *J* = 7.5 Hz, 4H), 6.91 (d, *J* = 11.7 Hz, 4H), 5.58 (s, 4H), 3.19 (t, *J* = 7.7

Hz, 4H), 2.67 – 2.59 (m, 4H), 1.95 (m, 4H), 1.60 (m, 4H), 1.34 (m, 44H), 0.95 (m, 12H).

12,13-bis(4-hexylbenzyl)-3,9-diundecyl-12,13-dihydro-[1,2,5]thiadiazolo[3,4-e]thieno[2",3":4',5']thieno[2',3':4,5]pyrrolo[3,2-g]thieno[2',3':4,5]thieno[3,2-b]indole-2,10-dicarbaldehyde (4c)

Compound **3a** was replaced with compound **3c** (470 mg, 92%). ^{1}H NMR (400 MHz, CDCl$_3$), δ (ppm): 9.97 (s, 2H), 7.16 – 7.11 (d, *J* = 7.9 Hz, 4H), 6.90 (d, *J* = 7.9 Hz, 4H), 5.47 (s, 4H), 3.09 (t, *J* = 7.7 Hz, 4H), 2.65 (t, *J* = 7.7 Hz, 4H), 1.85 (m, 4H), 1.64 (m, 4H), 1.44 – 1.19 (m, 44H), 0.94 – 0.83 (m, 12H).

2,2′-((2Z,2′Z)-((12,13-bis(2-hexylbenzyl)-3,9-diundecyl-12,13-dihydro-[1,2,5]thiadiazolo[3,4-*e*]thieno[2″,3″:4′,5′]thieno[2′,3′:4,5]pyrrolo[3,2-*g*]thieno[2′,3′:4,5]thieno[3,2-*b*]indole-2,10-diyl)bis(methaneylylidene))bis(5,6-difluoro-3-oxo-2,3-dihydro-1*H*-indene-2,1-diylidene))dimalononitrile (*o*-BzY)

Compound **4a** (450 mg, 0.39 mmol) and 2-(5,6-difluoro-3-oxo-2,3-dihydro-1*H*-inden-1-ylidene)malononitrile (424.7 mg, 1.87 mmol) were added pyridine (1.5 mL) in 45 mL of chloroform. The mixture was stirred at 70 °C overnight. After cooling to room temperature, the reaction mixture was quenched with water, extracted with brine and chloroform, and dried over magnesium sulfate. After concentrating the reaction mixture under reduced pressure, the residue was purified by column chromatography with hexane and chloroform, yielding a dark blue solid (0.52 g, 85%). ^{1}H NMR (400 MHz, CDCl$_3$), δ (ppm): 8.70 (s, 2H), 8.38 (dd, *J* = 9.9, 6.4 Hz, 2H), 7.53 (t, *J* = 7.5 Hz, 2H), 7.38 (d, *J* = 4.1 Hz, 4H), 7.15 (d, *J* = 20.1 Hz, 4H), 5.57 (s, 4H), 2.94 (t, *J* = 7.8 Hz, 4H), 2.05 (t, *J* = 8.1 Hz, 4H), 1.68 (m, 8H), 1.49 – 1.17 (m, 44H), 0.97 – 0.80 (m, 12H). ^{13}C NMR (100 MHz, CDCl$_3$), δ (ppm): 185.17, 158.21, 153.14, 147.18, 145.04, 140.60, 137.41, 135.15, 134.38, 134.35, 134.31, 133.61, 132.78, 132.28, 130.07, 129.72, 128.73, 126.72, 124.70, 119.79, 119.77, 114.74, 114.48, 113.21, 99.99, 68.29, 51.83, 31.94, 31.89, 31.73, 31.05, 29.80, 29.75, 29.66, 29.65, 29.52, 29.46, 29.44, 29.36, 22.84, 22.71, 14.24, 14.15.

2,2′-((2Z,2′Z)-((12,13-bis(3-hexylbenzyl)-3,9-diundecyl-12,13-dihydro-[1,2,5]thiadiazolo[3,4-*e*]thieno[2″,3″:4′,5′]thieno[2′,3′:4,5]pyrrolo[3,2-*g*]thieno[2′,3′:4,5]thieno[3,2-*b*]indole-2,10-diyl)bis(methaneylylidene))bis(5,6-difluoro-3-oxo-2,3-dihydro-1*H*-indene-2,1-diylidene))dimalononitrile (*m*-BzY)

Compound **4a** was replaced with compound **4b** (0.52 g, 85%). ^{1}H NMR (400 MHz, CDCl$_3$), δ (ppm): 8.55 (s, 2H), 8.38 (dd, *J* = 9.9, 6.5 Hz, 2H), 7.43 (t, *J* = 7.7 Hz, 2H), 7.27 (t, *J* = 7.7 Hz, 2H), 7.17 (d, *J* = 7.7 Hz, 2H), 6.93 (d, *J* = 7.8 Hz, 2H), 6.88 (t, *J* = 1.7 Hz, 2H), 5.57 (s, 4H), 2.86 (t, *J* = 8.0 Hz, 4H), 2.55 (t, *J* = 7.8 Hz, 4H), 1.67 (m, 4H), 1.54 – 1.12 (m, 48H), 0.91 – 0.75 (m, 12H). ^{13}C NMR (100 MHz, CDCl$_3$), δ (ppm): 185.39, 153.30, 147.05, 146.38, 145.13, 144.27, 137.73, 134.85, 134.57, 134.08, 134.06, 134.00, 133.98, 133.27, 132.96, 130.47, 129.23, 128.79, 125.97, 122.88, 119.48, 114.56, 114.44, 113.41, 99.99, 68.78, 53.97, 35.92, 31.96, 31.76, 31.26, 30.88, 29.79, 29.67, 29.66, 29.53, 29.42, 29.38, 29.05, 22.73, 22.64, 14.16, 14.09.

2,2′-((2Z,2′Z)-((12,13-bis(4-hexylbenzyl)-3,9-diundecyl-12,13-dihydro-[1,2,5]thiadiazolo[3,4-*e*]thieno[2″,3″:4′,5′]thieno[2′,3′:4,5]pyrrolo[3,2-*g*]thieno[2′,3′:4,5]thieno[3,2-*b*]indole-2,10-diyl)bis(methaneylylidene))bis(5,6-difluoro-3-oxo-2,3-dihydro-1*H*-indene-2,1-diylidene))dimalononitrile (*p*-BzY)

Compound **4a** was replaced with compound **4c** (0.52 g, 84%). ^{1}H NMR (400 MHz, $CDCl_3$), δ (ppm): 8.54 (s, 2H), 8.38 (dd, *J* = 9.9, 6.5 Hz, 2H), 7.41 (t, *J* = 7.5 Hz, 2H), 7.18 (d, *J* = 8.0 Hz, 4H), 7.00 (d, *J* = 8.0 Hz, 4H), 5.55 (s, 4H), 2.86 (t, *J* = 8.0 Hz, 4H), 2.61 (t, *J* = 7.8 Hz, 4H), 1.71 – 1.57 (m, 8H), 1.40 – 1.17 (m, 44H), 0.91 – 0.78 (m, 12H). ^{13}C NMR (100 MHz, $CDCl_3$), δ (ppm): 185.41, 153.32, 152.68, 147.03, 145.12, 143.57, 137.68, 134.85, 134.06, 133.94, 133.24, 132.92, 131.79, 130.42, 129.41, 125.75, 119.45, 114.58, 114.45, 113.39, 111.69, 102.91, 68.82, 53.77, 35.74, 31.96, 31.75, 31.40, 30.89, 29.80, 29.67, 29.66, 29.53, 29.42, 29.38, 29.04, 22.73, 22.64, 14.16, 14.07.

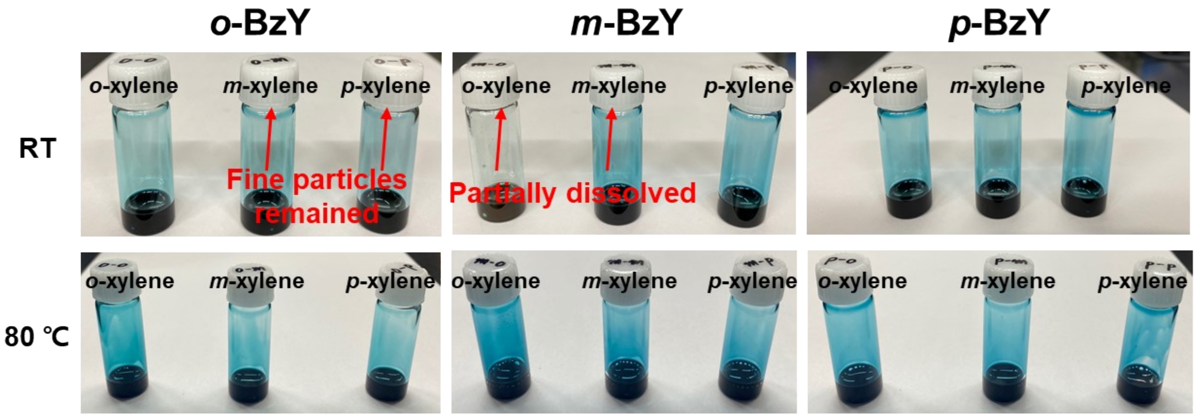

Fig. S1 The solutions of BzY-series in ***o***-xylene, *m*-xylene, and *p*-xylene at room temperature and 80 °C.

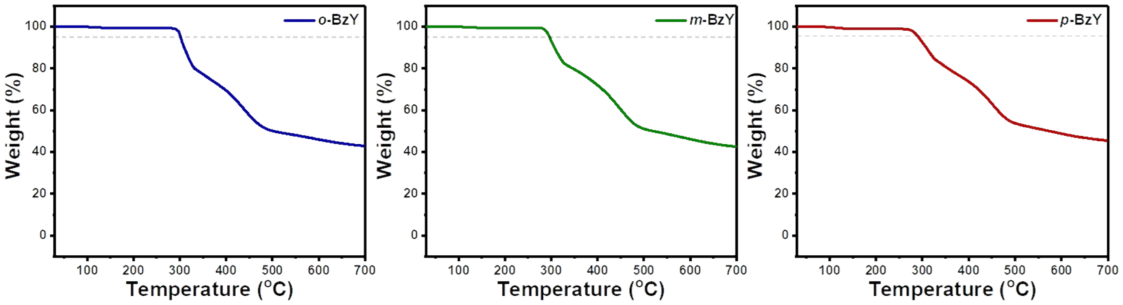

Fig. S2 TGA thermograms of *o*-BzY, *m*-BzY, and *p*-BzY.

Table S1 TGA thermal parameters of *o*-BzY, *m*-BzY, and *p*-BzY.

	***o*-BzY**	***m*-BzY**	***p*-BzY**
T_{5d} [°C]	302	296	292

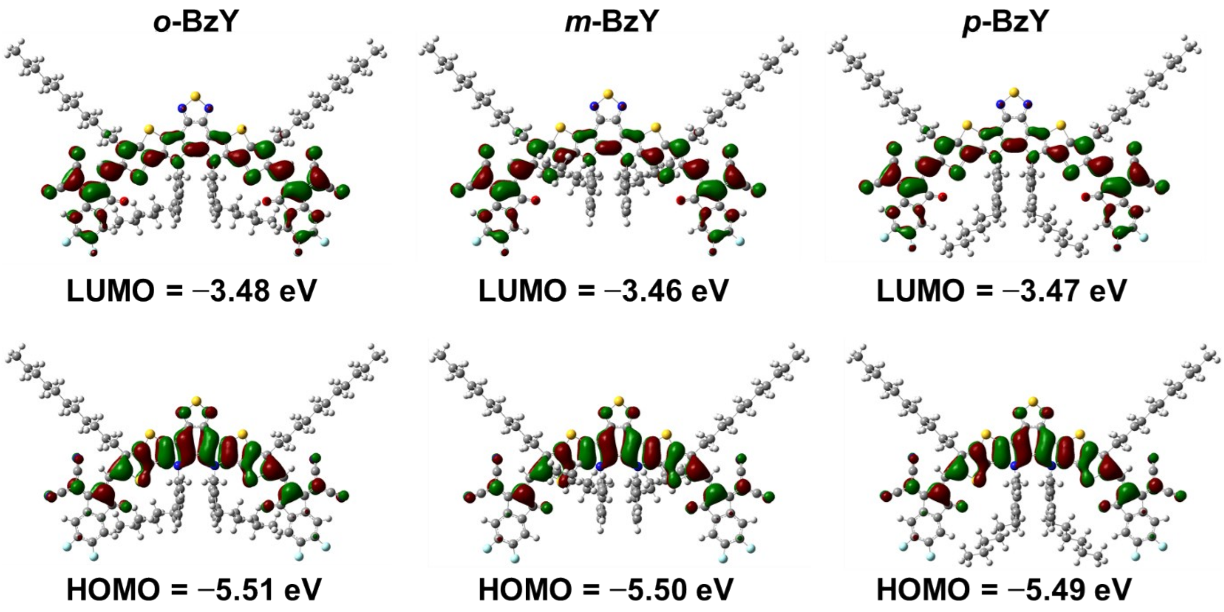

Fig. S3 Distribution of HOMO and LUMO wave functions and calculated energy levels of NFAs.

Table S2. Calculated dipole moments of *o*-BzY, *m*-BzY, and *p*-BzY.

	Vector			**Dipole Moment [D]**
	x	**y**	**z**	
***o*-BzY**	0.0003	2.6040	-0.0015	2.6040
***m*-BzY**	0.0001	2.0448	0.0001	2.0448
***p*-BzY**	0.0002	3.1484	-0.0010	3.1484

Fig. S4. Structure of hexylbenzene and its dipole moment direction.

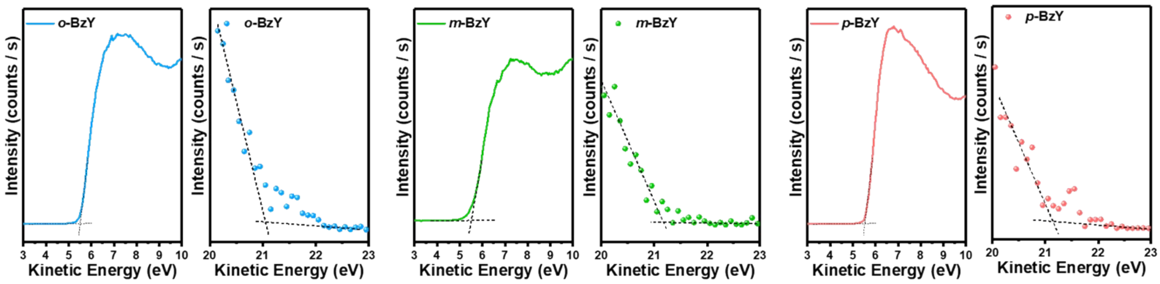

Fig. S5. UPS (He I; hv` = 21.22 eV) data of BzY-series NFAs’ films.

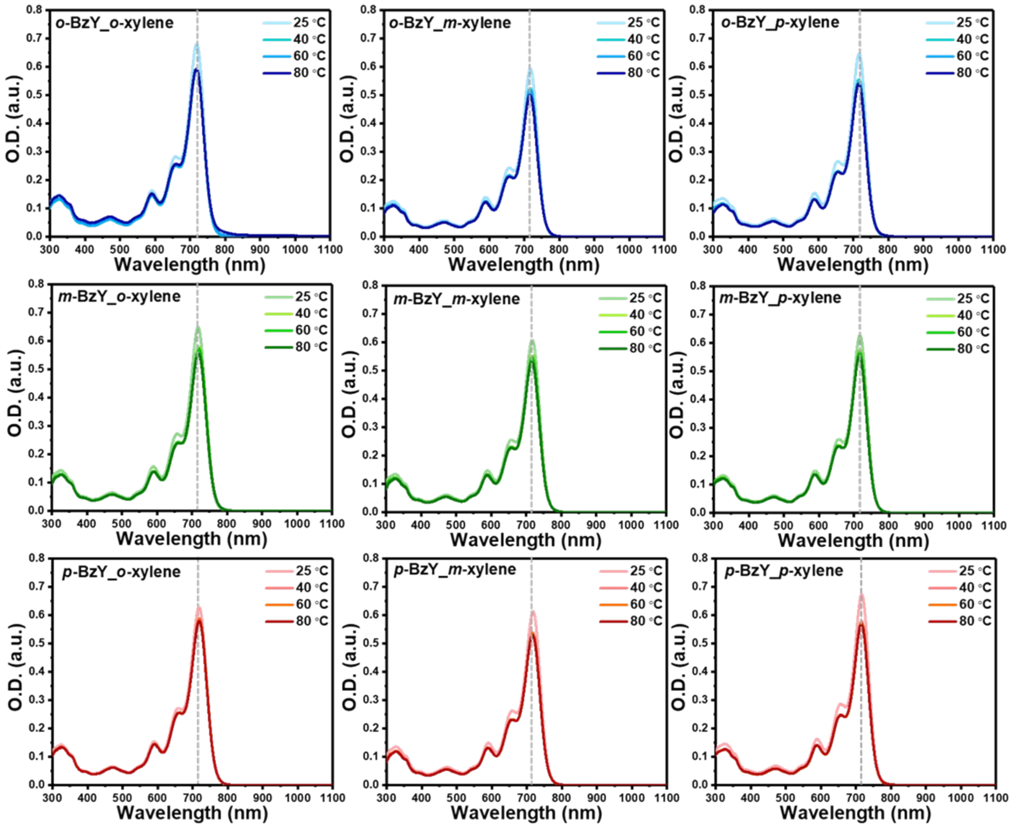

Fig. S6 Temperature-dependent UV-vis absorption spectra of *o*-BzY, *m*-BzY, and *p*-BzY in *o*-xylene, *m*-xylene, and *p*-xylene.

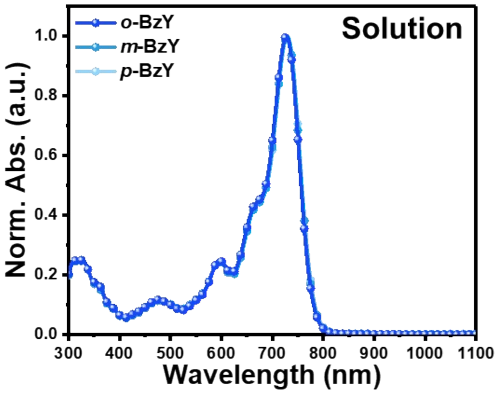

Fig. S7 UV-vis absorption spectra of *o*-BzY, *m*-BzY, and *p*-BzY in chloroform solution.

Table S3 Optical properties of *o*-BzY, *m*-BzY, and *p*-BzY in chloroform solution and corresponding thin-films.

	λ_{sol}^{max} [nm][a]	λ_{film}^{max} [nm][a]	λ_{onset} [nm][b]	E_g^{opt} [eV][b]
o-BzY	728	773	846	1.49
m-BzY	729	788	871	1.45
p-BzY	730	785	868	1.45

[a]Taken from the material solutions in xylenes and corresponding films on glass substrates. [b]Determined from the onset of the UV-vis absorption plots in the films.

Table S4 Solvatochromic shifts of BzY-series NFAs.

NFAs	Processing solvent	λ_{sol}^{max} [nm][a]	ν [cm^{-1}][b]	Δν [cm^{-1}][b]
o-BzY	Chloroform	728	13736	211
	p-xylene	717	13947	
m-BzY	Chloroform	729	13717	211
	p-xylene	718	13928	
p-BzY	Chloroform	730	13699	229
	p-xylene	718	13928	

[a]Taken from the material solutions in xylenes and corresponding films on glass substrates. [b]Calculated by the equation of *v* (wavenumber) [cm^{-1}] = 1/(λ (wavelength) [nm]).

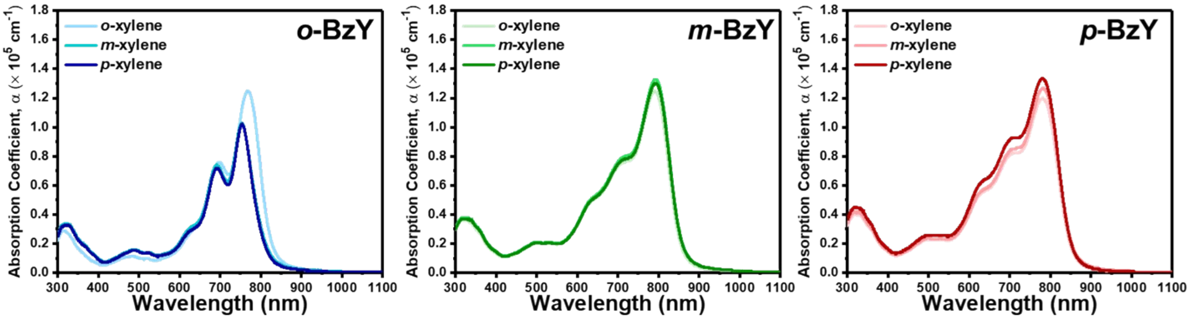

Fig. S8 Absorption coefficient of neat films of NFAs prepared by three kinds of xylene.

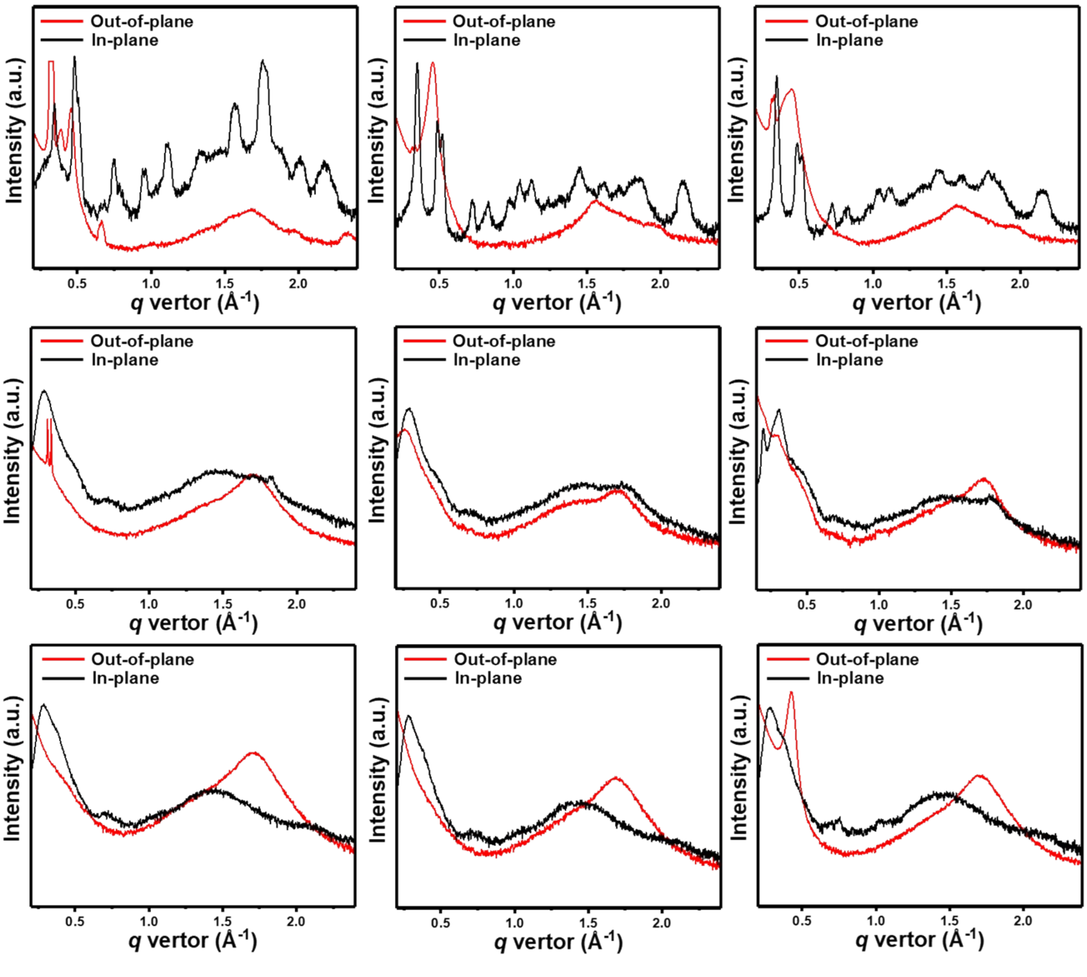

Fig. S9 Line-cut profiles of *o*-BzY prepared by (a) *o*-, (b) *m*-, and (c) *p*-xylene, *m*-BzY prepared by (d) *o*-, (e) *m*-, and (f) *p*-xylene, and *p*-BzY neat films prepared by (a) *o*-, (b) *m*-, and (c) *p*-xylene.

Table S5 GIWAXS parameters of *o*-BzY, *m*-BzY, and *p*-BzY neat films prepared by *o*-, *m*-, and *p*-xylene.

	Out-of-plane			In-plane		
	π-π staking			Lamella stacking		
	q [Å^{-1}]	*d*-spacing [Å]	Coherence length [Å]	*q* [Å^{-1}]	*d*-spacing [Å]	Coherence length [Å]
o-BzY (OX)	Polycrystalline			Polycrystalline		
o-BzY (MX)						
o-BzY (PX)						
m-BzY (OX)	1.71	3.675	25.281	0.286	21.995	66.439
m-BzY (MX)	1.725	3.642	26.782	0.285	22.031	66.572
m-BzY (PX)	1.729	3.634	34.640	0.299	20.996	70.027
p-BzY (OX)	1.713	3.668	21.78	0.279	22.518	83.123
p-BzY (MX)	1.692	3.714	21.519	0.275	22.821	85.42
p-BzY (PX)	1.705	3.686	22.511	0.275	22.828	85.137

Table S6. Vapor pressure and boiling point of *o*-xylene, *m*-xylene, and *p*-xylene.[1]

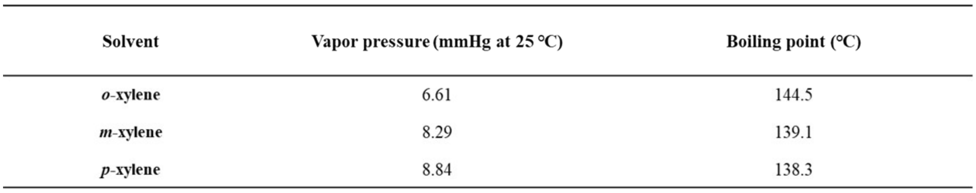

Solvent	Vapor pressure (mmHg at 25 °C)	Boiling point (°C)
***o*-xylene**	6.61	144.5
***m*-xylene**	8.29	139.1
***p*-xylene**	8.84	138.3

Table S7 Change in chemical shifts of H_1−H_4 in BzY-series NFAs as elevating temperatures.

NFA	Peak	Changes in temperature	Change in chemical shifts [ppm]			
			$CDCl_3$	*o*-xylene-d_{10}[a]	*m*-xylene-d_{10}[a]	*p*-xylene-d_{10}
o-BzY	H_1	RT − 50 ℃	0.07	0.02	0.02	0.01
		50 ℃ − 80 ℃	-	0.03	0.03	0.04
	H_2	RT − 50 ℃	0.03	0.03	0.02	0.03
		50 ℃ − 80 ℃	-	0.02	0.03	0.03
	H_3	RT − 50 ℃	0.04	0.10	0.09	0.12
		50 ℃ − 80 ℃	-	0.11	0.10	0.10
	H_4	RT − 50 ℃	0.05	0.01	0.01	0.01
		50 ℃ − 80 ℃	-	0.00	0.00	0.01
m-BzY	H_1	RT − 50 ℃	0.10	-	-	0.09
		50 ℃ − 80 ℃	-	0.06	0.08	0.08
	H_2	RT − 50 ℃	0.04	-	-	0.03
		50 ℃ − 80 ℃	-	0.03	0.03	0.03
	H_3	RT − 50 ℃	0.05	-	-	0.04
		50 ℃ − 80 ℃	-	0.05	0.04	0.04
	H_4	RT − 50 ℃	0.07	-	-	0.01
		50 ℃ − 80 ℃	-	0.02	0.02	0.02
p-BzY	H_1	RT − 50 ℃	0.10	0.08	0.10	0.09

		50 °C – 80 °C	-	0.07	0.09	0.10
	H_2	RT – 50 °C	0.03	0.03	0.03	0.04
		50 °C – 80 °C	-	0.03	0.03	0.03
	H_3	RT – 50 °C	0.05	0.04	0.04	0.05
		50 °C – 80 °C	-	0.06	0.05	0.05
	H_4	RT – 50 °C	0.06	0.00	0.01	0.02
		50 °C – 80 °C	-	0.01	0.01	0.02

[a] The *m*-BzY data in *o*-xylene-d_{10} and *m*-xylene-d_{10} at RT were excluded because of low solubility of m-BzY in those solvents.

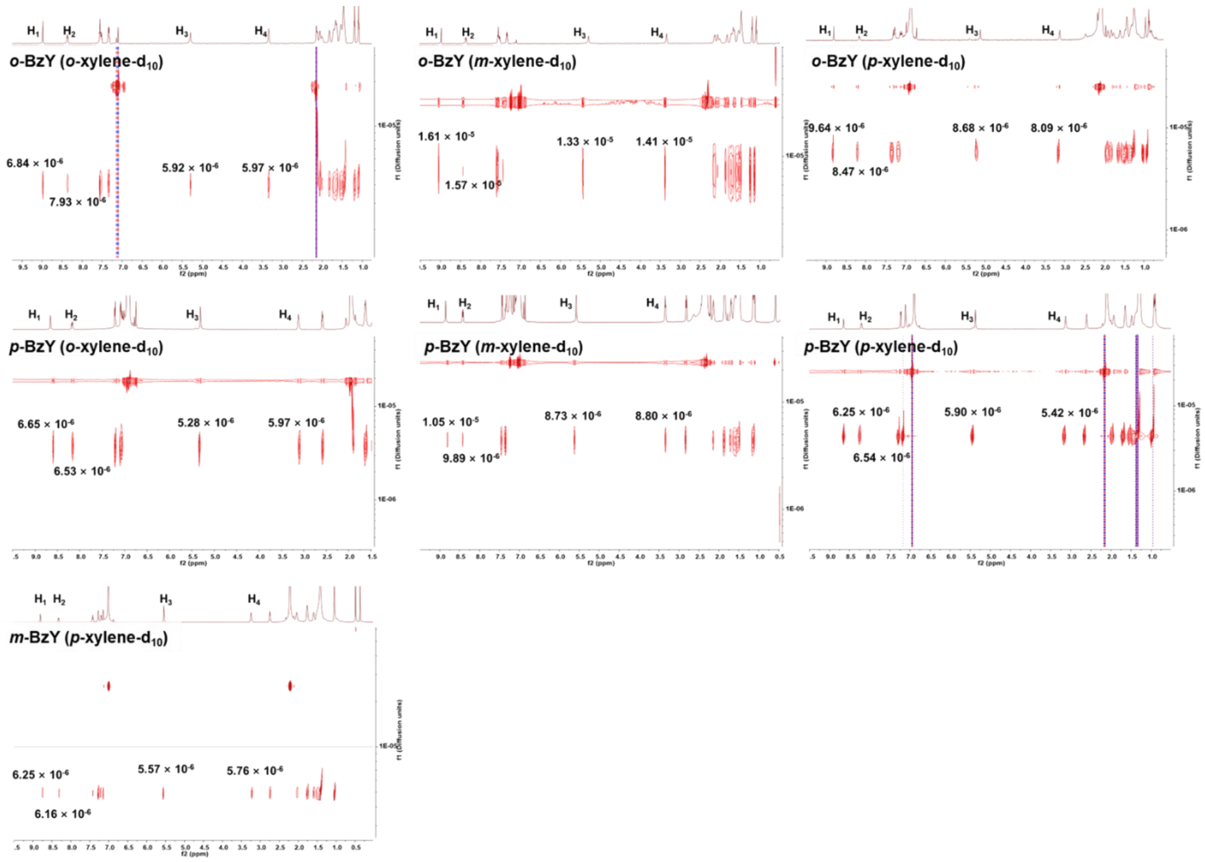

Fig. S10 DOSY NMR spectra of *o*-BzY and *p*-BzY in *o*-xylene-d_{10}, *m*-xylene-d_{10}, and *p*-xylene-d_{10} and *m*-BzY in *p*-xylene-d_{10}.

Table S8 Diffusion coefficients of NFAs in deuterated *o*-xylene, *m*-xylene, and *p*-xylene solutions.

NFA	Solvent	Diffusion coefficient [$cm^2 s^{-1}$]					
		H_1	H_2	H_3	H_4	Proton in solvent molecule	
						In aromatic	In methyl
***o*-BzY**	*o*-xylene-d_{10}	6.84×10^{-6} ($\pm 1.84 \times 10^{-7}$)	7.93×10^{-6} ($\pm 2.00 \times 10^{-7}$)	5.92×10^{-6} ($\pm 1.41 \times 10^{-7}$)	5.97×10^{-6} ($\pm 1.18 \times 10^{-7}$)	1.86×10^{-5} ($\pm 4.66 \times 10^{-9}$)	1.82×10^{-5} ($\pm 1.82 \times 10^{-8}$)
	m-xylene-d_{10}	1.61×10^{-5} ($\pm 2.70 \times 10^{-7}$)	1.57×10^{-5} ($\pm 3.27 \times 10^{-7}$)	1.33×10^{-5} ($\pm 2.21 \times 10^{-7}$)	1.41×10^{-5} ($\pm 2.41 \times 10^{-7}$)	2.66×10^{-5} ($\pm 7.05 \times 10^{-8}$)	2.66×10^{-5} ($\pm 7.14 \times 10^{-8}$)
	p-xylene-d_{10}	9.64×10^{-6} ($\pm 2.96 \times 10^{-7}$)	8.47×10^{-6} ($\pm 2.40 \times 10^{-7}$)	8.68×10^{-6} ($\pm 2.28 \times 10^{-7}$)	8.09×10^{-6} ($\pm 2.37 \times 10^{-7}$)	2.46×10^{-5} ($\pm 3.02 \times 10^{-8}$)	2.46×10^{-5} ($\pm 1.74 \times 10^{-8}$)
***m*-BzY**	*o*-xylene-d_{10}	-	-	-	-	-	-
	m-xylene-d_{10}	-	-	-	-	-	-
	p-xylene-d_{10}	6.25×10^{-6} ($\pm 1.18 \times 10^{-7}$)	6.16×10^{-6} ($\pm 1.17 \times 10^{-7}$)	5.75×10^{-6} ($\pm 1.06 \times 10^{-7}$)	5.76×10^{-6} ($\pm 1.12 \times 10^{-7}$)	2.44×10^{-5} ($\pm 2.30 \times 10^{-8}$)	2.45×10^{-5} ($\pm 2.09 \times 10^{-8}$)
***p*-BzY**	*o*-xylene-d_{10}	6.65×10^{-6} ($\pm 2.43 \times 10^{-7}$)	6.53×10^{-6} ($\pm 2.86 \times 10^{-7}$)	5.28×10^{-6} ($\pm 1.33 \times 10^{-7}$)	5.97×10^{-6} ($\pm 1.93 \times 10^{-7}$)	1.87×10^{-5} ($\pm 8.10 \times 10^{-9}$)	1.82×10^{-5} ($\pm 2.31 \times 10^{-8}$)
	m-xylene-d_{10}	1.05×10^{-5} ($\pm 1.84 \times 10^{-7}$)	9.89×10^{-6} ($\pm 2.33 \times 10^{-7}$)	8.73×10^{-6} ($\pm 1.95 \times 10^{-7}$)	8.80×10^{-6} ($\pm 2.34 \times 10^{-7}$)	2.36×10^{-5} ($\pm 5.55 \times 10^{-9}$)	2.35×10^{-5} ($\pm 3.58 \times 10^{-9}$)
	p-xylene-d_{10}	6.25×10^{-6} ($\pm 1.22 \times 10^{-7}$)	6.54×10^{-6} ($\pm 1.41 \times 10^{-7}$)	5.90×10^{-6} ($\pm 1.18 \times 10^{-7}$)	5.42×10^{-6} ($\pm 9.12 \times 10^{-8}$)	2.43×10^{-5} ($\pm 2.79 \times 10^{-8}$)	2.45×10^{-5} ($\pm 1.75 \times 10^{-8}$)

Table S9. Photovoltaic performance of PM6:NFAs based solar cells with different conditions.

Active layer	D:A	V_{OC} [V][a]	J_{SC} [mA cm^{-2}][a]	FF [%][a]	PCE [%][a]
PM6:*o*-BzY (*o*-xylene)	1:1.2	0.90 (0.904±0.002)	23.0 (23.0±0.49)	64.8 (64.8±0.29)	13.5(13.5±0.21)
	1:1.3	0.91 (0.914±0.002)	23.3 (23.0±0.44)	64.8 (64.7±0.21)	13.8(13.6±0.21)
	1:1.5	0.92 (0.922±0.005)	23.8 (23.6±0.59)	65.6 (65.5±0.17)	14.4 (14.2±0.28)
PM6:*m*-BzY (*m*-xylene)	1:1.2	0.88 (0.880±0.005)	23.4 (23.3±0.36)	73.1 (72.4±1.15)	15.0 (14.8±0.16)
	1:1.3	0.88 (0.882±0.003)	24.3 (23.8±0.62)	74.0 (74.4±0.26)	15.8 (15.6±0.32)
	1:1.5	0.89 (0.886±0.003)	23.6 (23.6±0.17)	73.9 (73.6±0.50)	15.5 (15.4±0.16)
PM6:*p*-BzY (*p*-xylene)	1:1.2	0.89 (0.888±0.003)	24.2 (24.0±0.27)	71.3 (69.4±1.63)	15.4 (14.8±0.35)
	1:1.3	0.88 (0.885±0.002)	24.2 (23.8±0.45)	68.7 (68.5±0.56)	14.7 (14.5±0.23)
	1:1.5	0.88 (0.883±0.002)	23.5 (23.1±0.33)	67.8 (66.9±1.15)	14.0 (13.6±0.29)

[a] The average values and standard deviations in the parentheses are based on 10 devices.

Table S10 Summary of reported performances for organic solar cell devices with non-additive and non-annealing process.

Ref.	Active layer	Processing solvent	V_{OC} [V]	J_{SC} [mA cm^{-2}]	FF [%]	PCE [%]
2	PBFTT:IT-4Cl (binary)	Chlorobenzene	0.76	19.7	73.9	11.1
3	PFBDB-T:CDTTIC (binary)	Chlorobenzene	0.78	24.9	56.0	11.5
4	PBDB-T:IDTCN-O (binary)	1,2-Dichlorobenzene	0.91	20.0	73.2	13.3
5	DI3T-1F:PC$_{71}$BM (binary)	Chloroform	0.82	13.6	75.1	8.3
6	PM6:DCB-4F:PC$_{71}$BM (ternary)	Chloroform	1.00	16.8	66.5	11.2
7	PM6:Y6:IT-M (ternary)	Chloroform	0.86	26.9	68.7	15.8
8	PM6:BTP-ClBr1:BTP-2O-4Cl-C12 (ternary)	Chloroform	0.90	24.9	74.8	16.7
9	PM6:Y6-eC6-BO (binary)	Chloroform	0.85	26.4	77.4	17.3
		o-Xylene	0.84	25.7	75.5	16.4
10	PBDB-T:DNO15T (binary)	Chlorobenzene	0.89	19.0	63.6	10.7
11	PBDB-T:DDTC-4F (binary)	Chlorobenzene	0.88	21.8	63.6	12.2
12	PBDB-T:Y6:L5 (ternary)	Chloroform	0.87	27.8	71.0	17.1

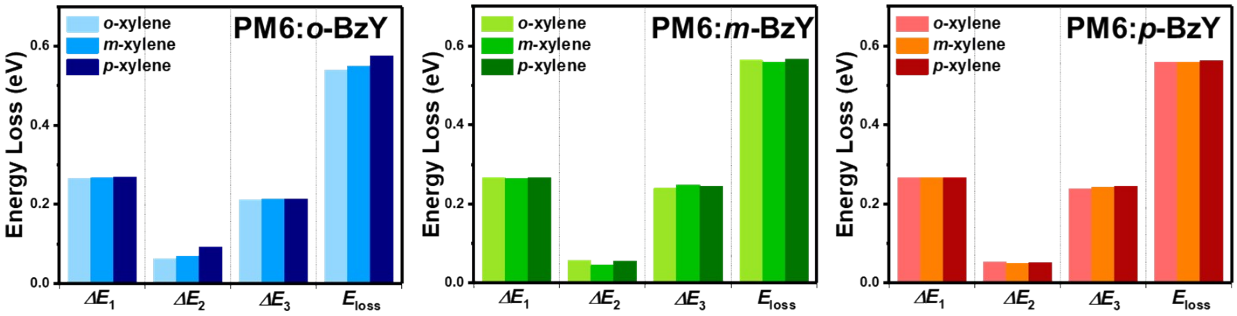

Fig. S11 Graphical illustration of energy losses of PM6:NFAs-based devices processed by three kinds of xylene.

Table S11. Detailed energy loss of the OSCs based on PM6:BzY-NFAs.

Active Layer	Solvent	E_g [eV]	qV_{OC} [eV]	E_{loss} [eV]	$\triangle E_1$ [eV]	$\triangle E_2$ [eV]	$\triangle E_3$ [eV]	EQE_{EL}
PM6:*o*-BzY	*o*-xylene	1.463	0.924	0.539	0.266	0.062	0.211	1.8×10^{-4}
	m-xylene	1.484	0.935	0.549	0.268	0.068	0.213	2.0×10^{-4}
	p-xylene	1.506	0.931	0.575	0.269	0.093	0.213	1.6×10^{-4}
PM6:*m*-BzY	*o*-xylene	1.445	0.881	0.564	0.266	0.058	0.240	8.0×10^{-5}
	m-xylene	1.447	0.888	0.559	0.265	0.045	0.249	6.8×10^{-5}
	p-xylene	1.453	0.886	0.567	0.266	0.056	0.245	8.0×10^{-5}
PM6:*p*-BzY	*o*-xylene	1.446	0.888	0.558	0.266	0.053	0.239	7.8×10^{-5}
	m-xylene	1.437	0.878	0.559	0.267	0.049	0.243	8.6×10^{-5}
	p-xylene	1.454	0.891	0.563	0.266	0.052	0.245	9.6×10^{-5}

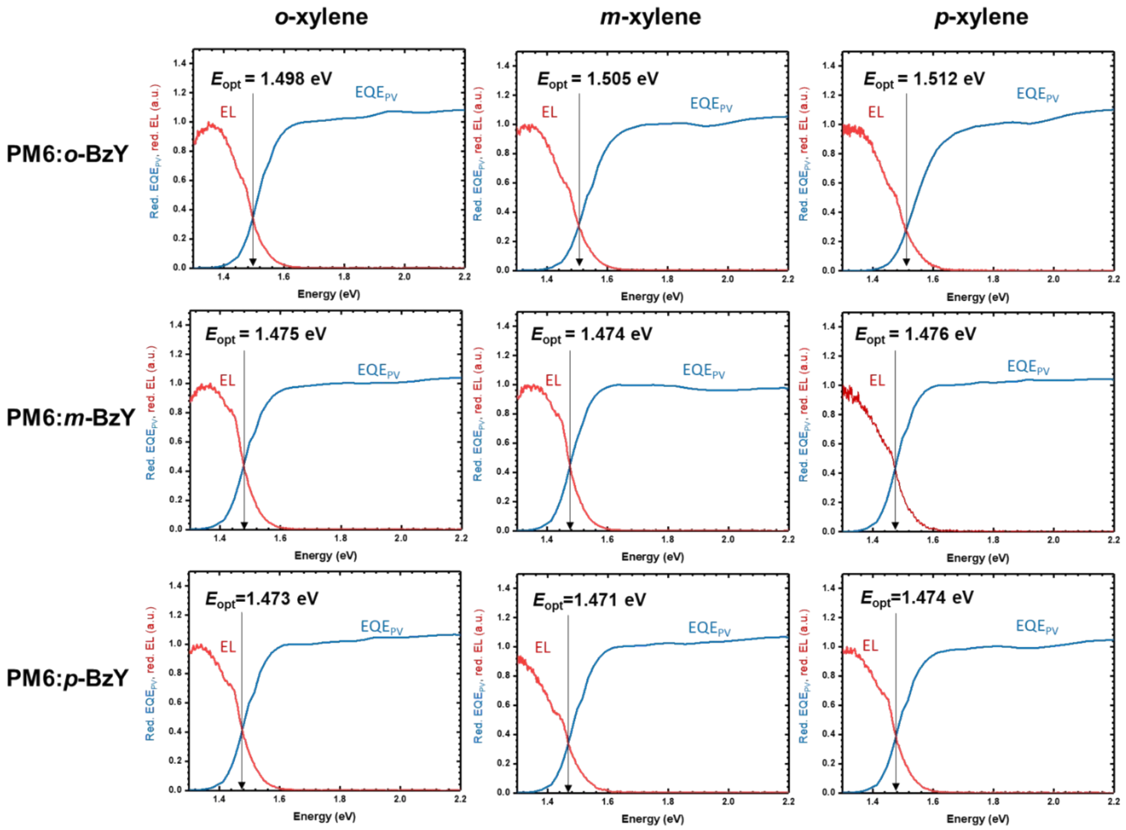

Fig. S12. Estimated optical bandgap of PM6:BzY-series NFAs blend films processed by *o*-xylene, *m*-xylene, and *p*-xylene using the crossing point between normalized EQE_{PV} and EL spectra.

Table S12 The charge dissociation and collection probabilities of BzY series-based devices.

Blend	**Processing solvent**	P_{diss}	P_{coll}
PM6:*o*-BzY	*o*-xylene	98.0%	86.0%
	m-xylene	92.5%	70.0%
	p-xylene	94.8%	71.9%
PM6:*m*-BzY	*o*-xylene	98.2%	86.7%
	m-xylene	99.3%	89.6%
	p-xylene	97.6%	84.4%
PM6:*p*-BzY	*o*-xylene	98.6%	85.1%
	m-xylene	98.8%	85.6%
	p-xylene	98.9%	85.3%

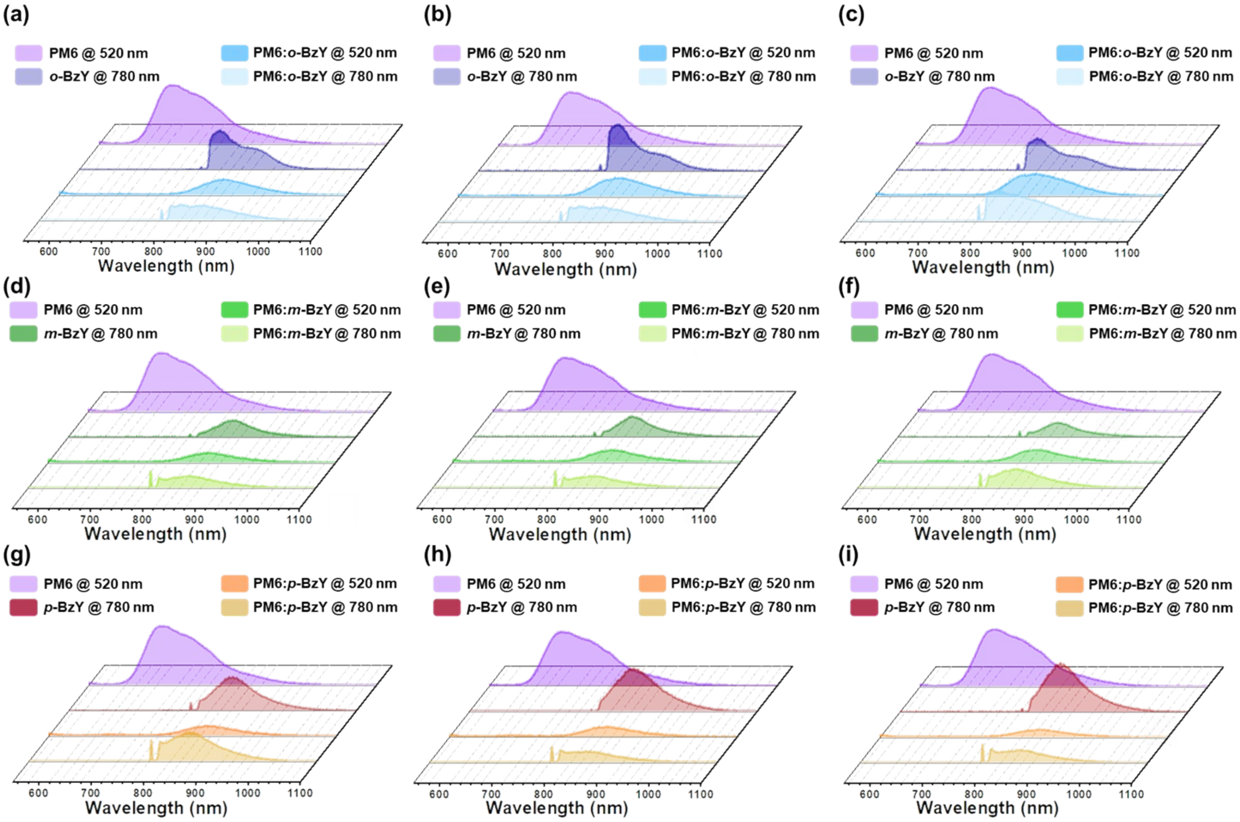

Fig. S13 Photoluminescence (PL) spectra of PM6, NFAs, and corresponding blend films prepared by (a), (d), and (g) *o*-xylene, (b), (e), and (b) *m*-xylene, and (c), (f), and (i) *p*-xylene.

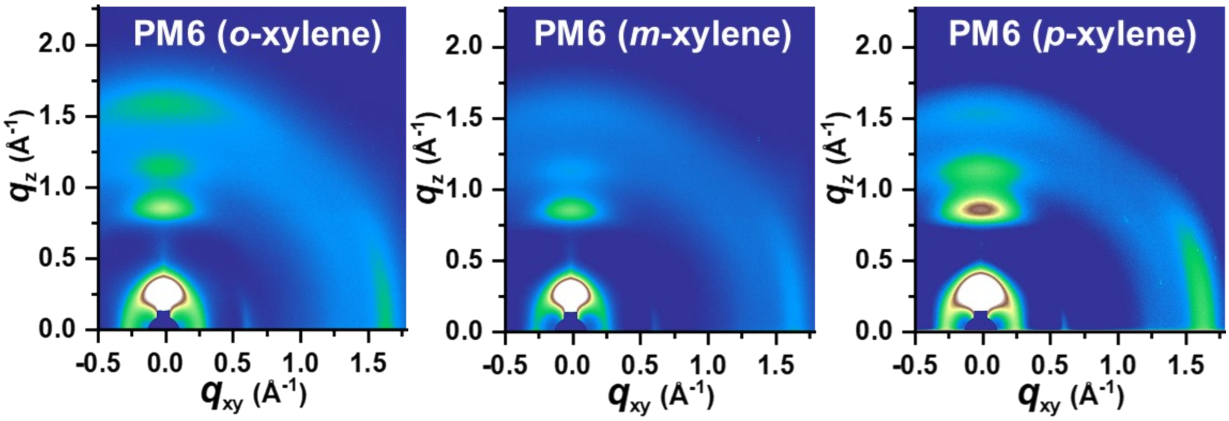

Fig. S14 2D GIWAXS images of PM6 prepared by *o*-xylene, *m*-xylene, and *p*-xylene.

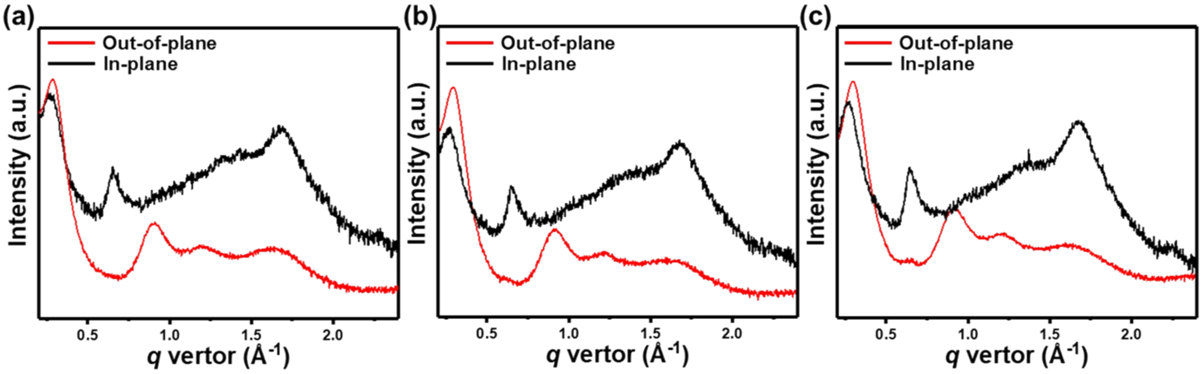

Fig. S15 Line-cut profiles of PM6 neat films prepared by (a) *o*-xylene, (b) *m*-xylene, and (c) *p*-xylene.

Table S13 GIWAXS parameters of PM6 neat films.

Processing Solvent	Out-of-plane						In-plane					
	π-π staking			Lamella stacking			π-π staking			Lamella stacking		
	q [Å^{-1}]	d-spacing [Å]	Coherence length [Å]	q [Å^{-1}]	d-spacing [Å]	Coherence length [Å]	q [Å^{-1}]	d-spacing [Å]	Coherence length [Å]	q [Å^{-1}]	d-spacing [Å]	Coherence length [Å]
o-xylene	1.635	3.842	22.107	0.281	22.337	73.026	1.694	3.710	38.797	0.265	23.737	69.660
m-xylene	1.647	3.815	20.596	0.290	21.671	72.933	1.680	3.740	36.499	0.261	24.097	44.377
p-xylene	1.609	3.904	22.853	0.296	21.238	77.917	1.676	3.750	28.882	0.264	23.768	47.680

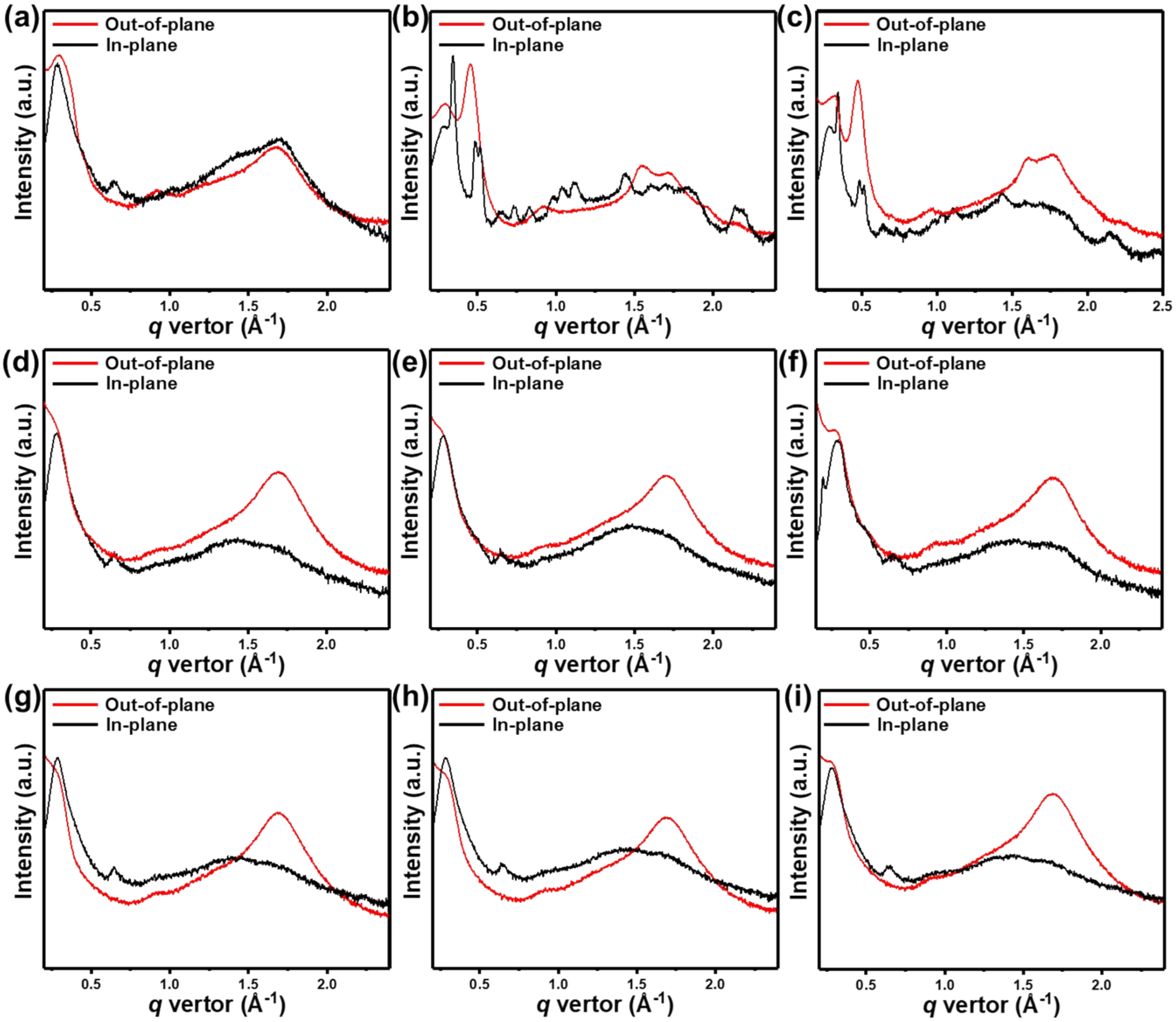

Fig. S16 Line-cut profiles of PM6:*o*-BzY prepared by (a) *o*-, (b) *m*-, and (c) *p*-xylene, PM6:*m*-BzY prepared by (d) *o*-, (e) *m*-, and (f) *p*-xylene, and PM6:*p*-BzY blend films prepared by (a) *o*-, (b) *m*-, and (c) *p*-xylene.

Table S14 GIWAXS parameters of PM6:*o*-BzY blend film prepared by *o*-xylene and PM6:*m*-BzY and PM6:*p*-BzY blend films prepared by *o*-, *m*-, and *p*-xylene..

	Out-of-plane						In-plane					
	π-π staking			Lamella stacking			π-π staking			Lamella stacking		
	q [Å^{-1}]	*d*-spacing [Å]	Coherence length [Å]	*q* [Å^{-1}]	*d*-spacing [Å]	Coherence length [Å]	*q* [Å^{-1}]	*d*-spacing [Å]	Coherence length [Å]	*q* [Å^{-1}]	*d*-spacing [Å]	Coherence length [Å]
PM6:*o*-BzY (OX)	1.681	3.737	29.206	0.287	21.911	41.767	1.714	3.667	29.657	0.282	22.316	78.520
PM6:*m*-BzY (OX)	1.696	3.704	29.939	0.262	23.963	62.130	1.701	3.693	40.597	0.280	22.475	81.413
PM6:*m*-BzY (MX)	1.710	3.675	31.354	0.258	24.387	55.853	1.717	3.659	34.403	0.282	22.302	77.403
PM6:*m*-BzY (PX)	1.694	3.708	28.983	0.272	23.109	55.927	1.716	3.661	37.059	0.285	22.077	71.117
PM6:*p*-BzY (OX)	1.696	3.706	26.422	0.276	22.775	67.864	1.697	3.702	41.796	0.283	22.226	93.467
PM6:*p*-BzY (MX)	1.696	3.704	30.613	0.282	22.269	64.308	1.704	3.687	40.103	0.281	22.382	88.578
PM6:*p*-BzY (PX)	1.692	3.713	30.814	0.272	23.061	54.901	1.683	3.734	43.406	0.279	22.505	88.772

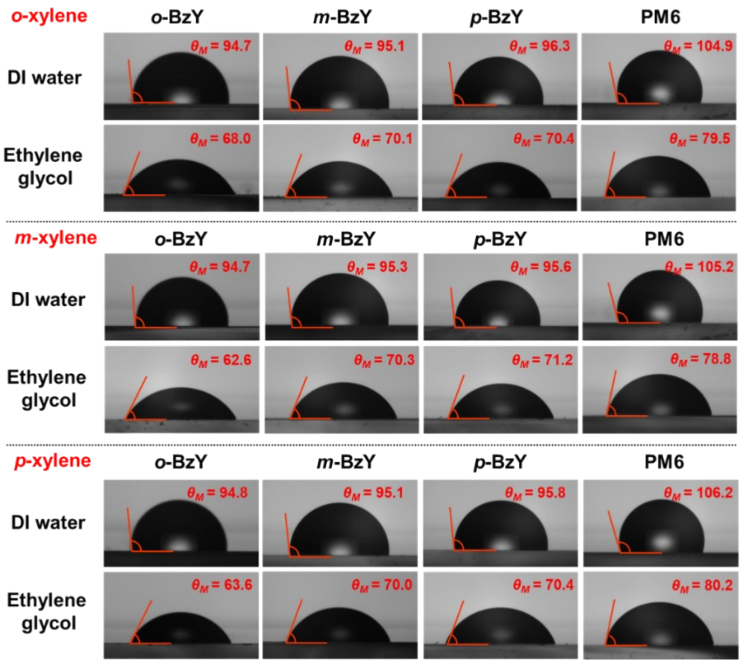

Fig. S17. Contact angles of *o*-BzY, *m*-BzY, *p*-BzY, and PM6 films processed by *o*-xylene, *m*-xylene, and *p*-

Table S15. Contact angle profiles, surface energies, and interaction parameters of BzY-series NFAs and PM6 films processed by *o*-, *m*-, and *p*-xylene.

NFA	Solvent	CA of water [°]	CA of Ethylene glycol [°]	Surface energy [mN/m]	Interaction parameter
***o*-BzY**	***o*-xylene**	**94.7**	**68.0**	**25.3**	**0.15**
	***m*-xylene**	**94.7**	**62.6**	**29.3**	**0.52**
	***p*-xylene**	**94.8**	**63.6**	**28.5**	**0.51**
***m*-BzY**	***o*-xylene**	**95.1**	**70.1**	**24.1**	**0.068**
	***m*-xylene**	**95.3**	**70.3**	**24.1**	**0.048**
	***p*-xylene**	**95.1**	**70.0**	**24.3**	**0.092**
***p*-BzY**	***o*-xylene**	**96.3**	**70.4**	**24.2**	**0.074**
	***m*-xylene**	**95.6**	**71.2**	**23.7**	**0.032**
	***p*-xylene**	**95.8**	**70.4**	**24.1**	**0.080**
PM6	***o*-xylene**	**104.9**	**79.5**	**21.6**	-
	***m*-xylene**	**105.2**	**78.8**	**22**	-
	***p*-xylene**	**106.2**	**80.2**	**21.4**	-

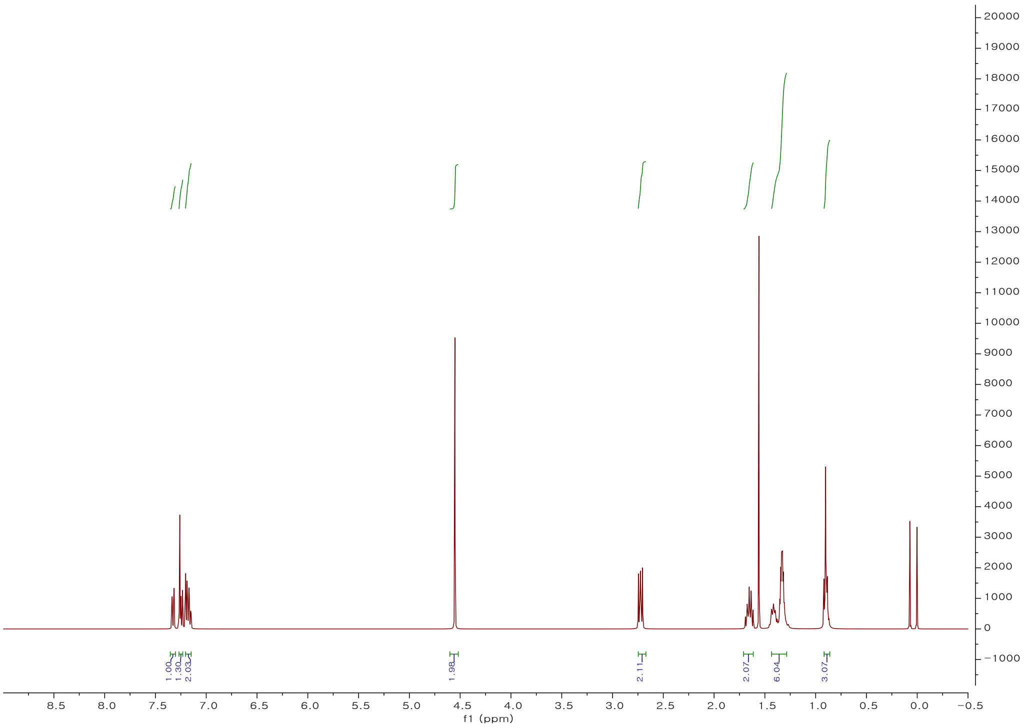

Fig. S18 ^{1}H NMR spectra of compound 1a in $CDCl_3$.

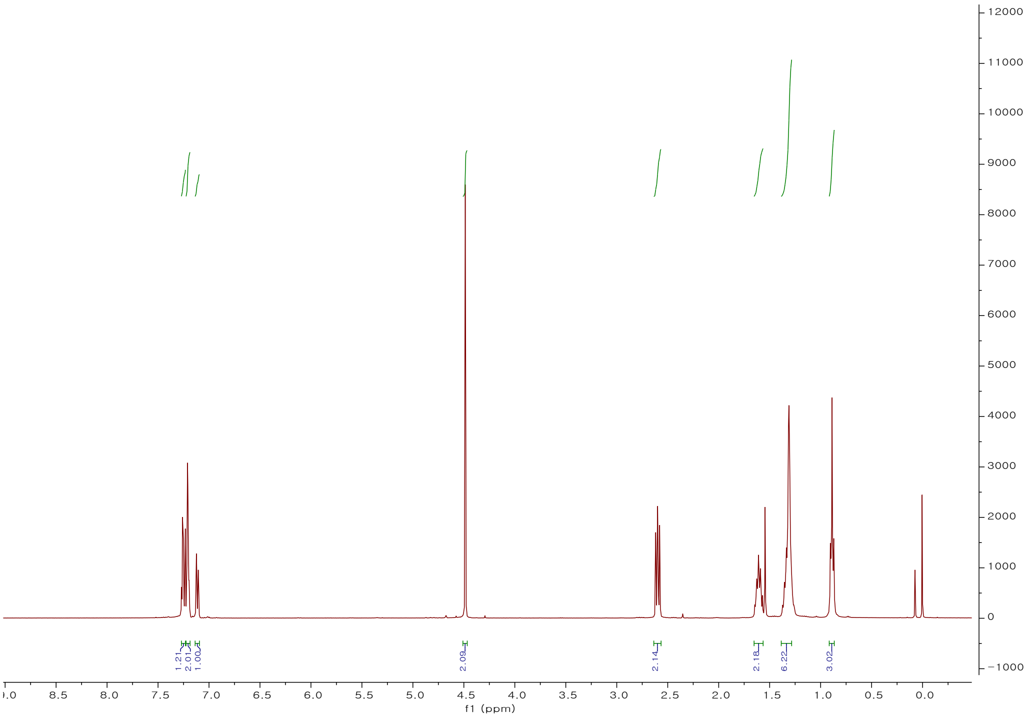

Fig. S19 ^{1}H NMR spectra of compound 1b in CDCl$_3$.

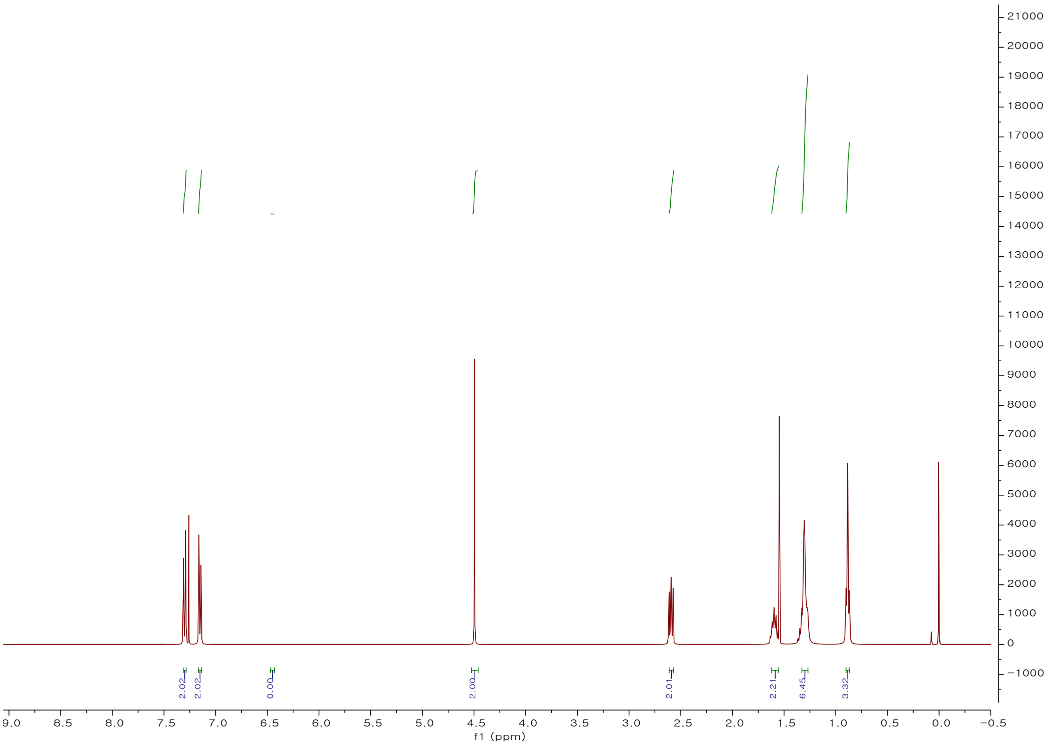

Fig. S20 ^{1}H NMR spectra of compound 1c in CDCl$_3$.

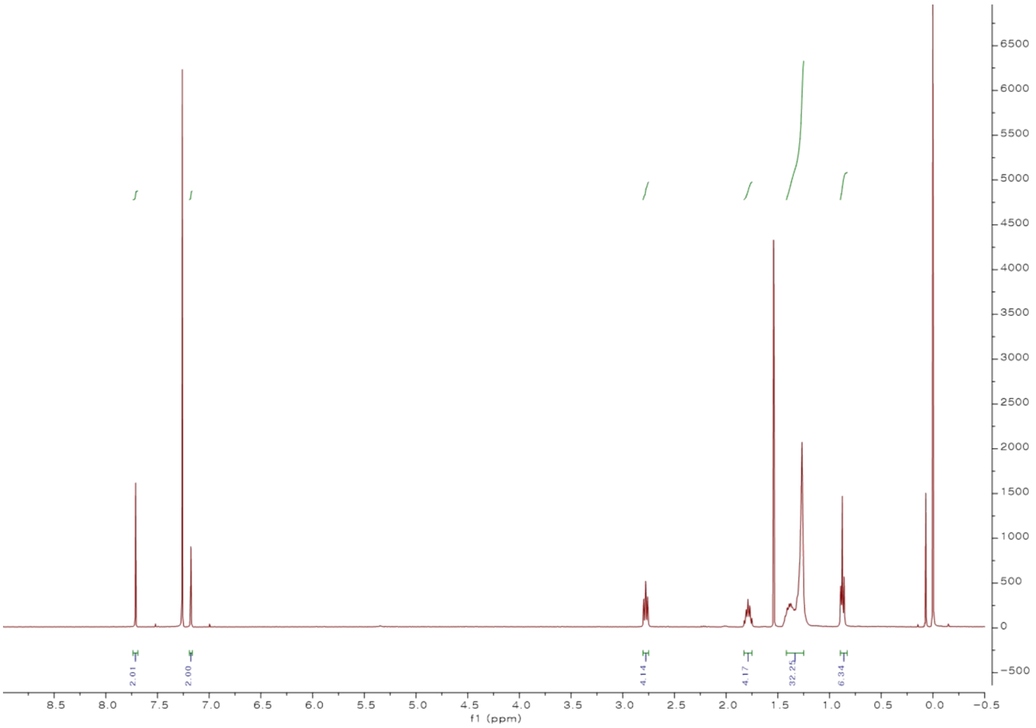

Fig. S21 ^{1}H NMR spectra of compound 2 in CDCl$_3$.

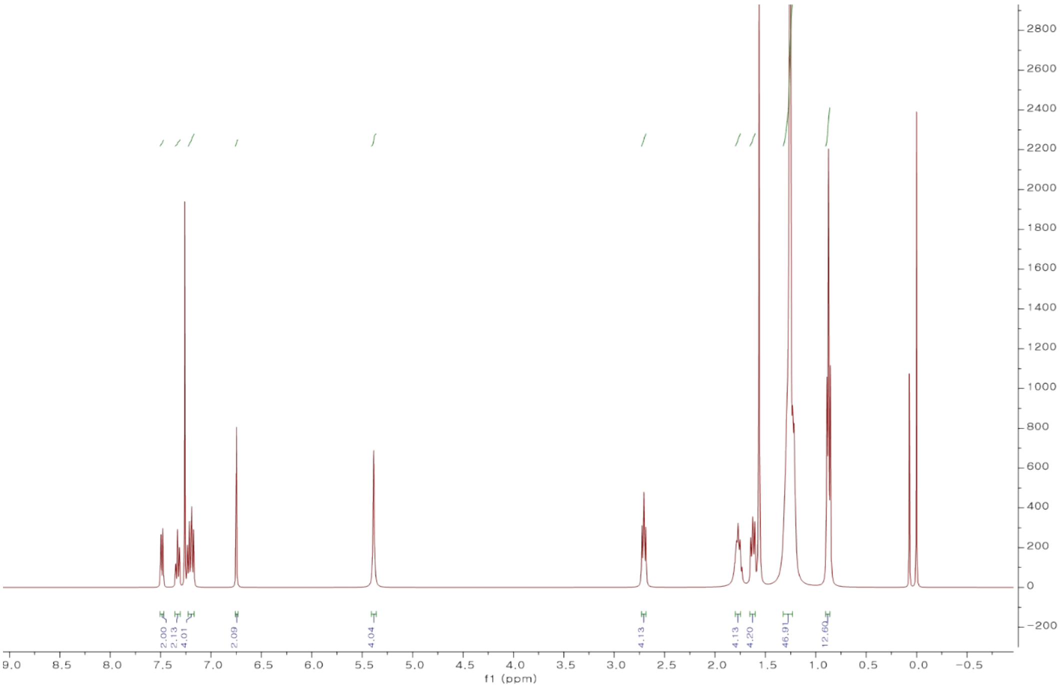

Fig. S22 ^{1}H NMR spectra of compound 3a in CDCl$_3$.

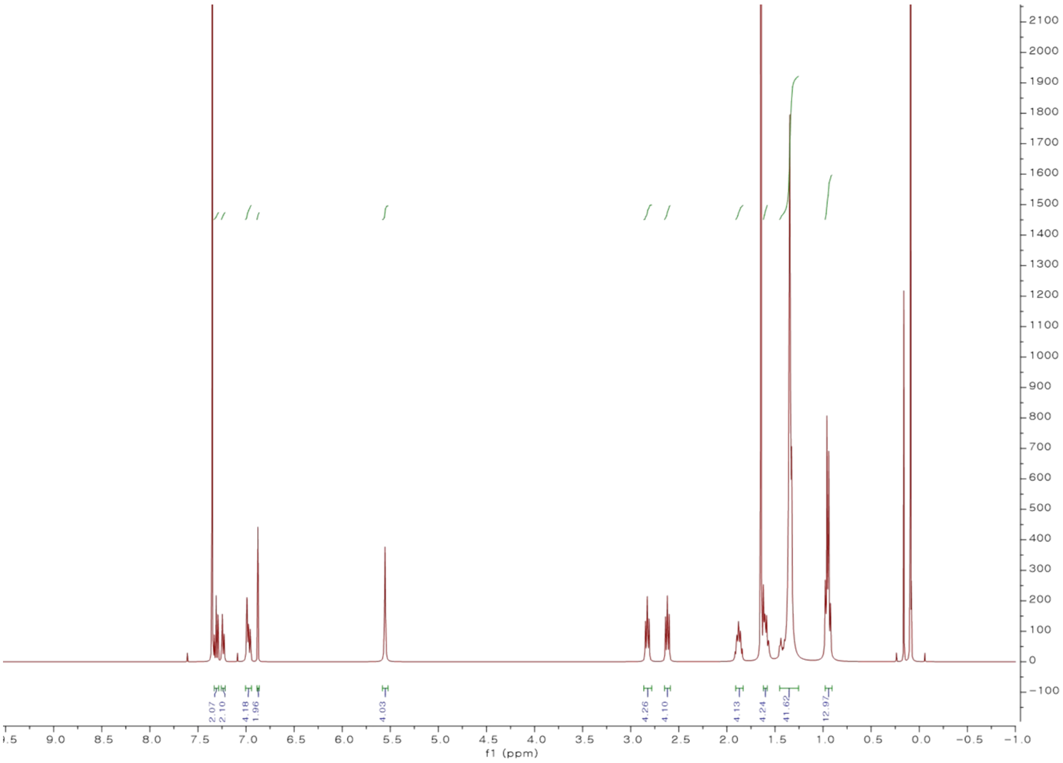

Fig. S23 ^{1}H NMR spectra of compound 3b in $CDCl_3$.

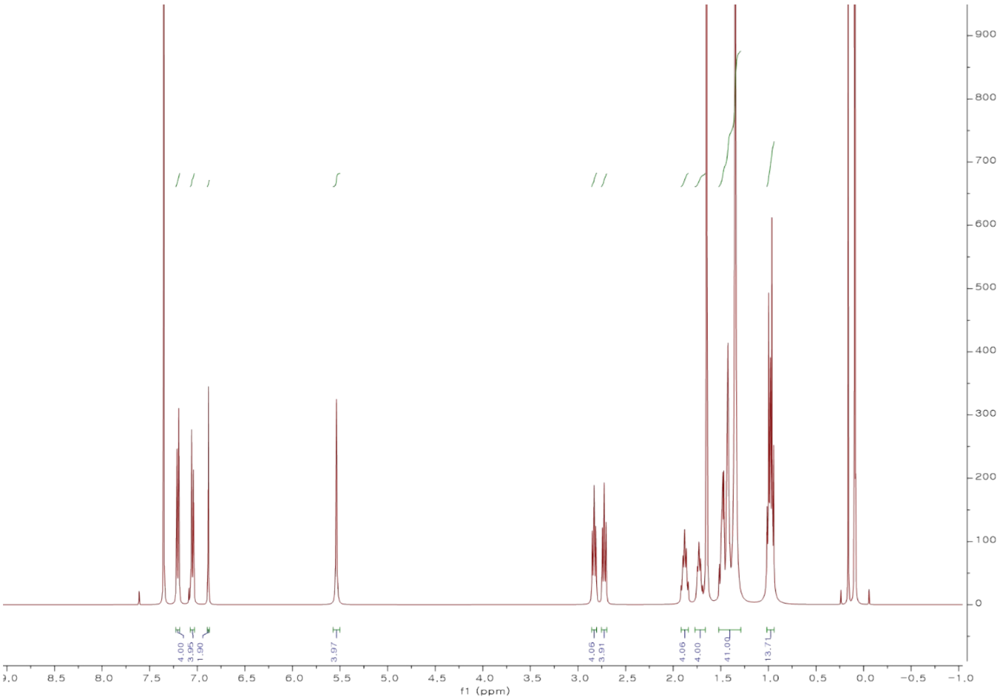

Fig. S24 ^{1}H NMR spectra of compound 3c in $CDCl_3$.

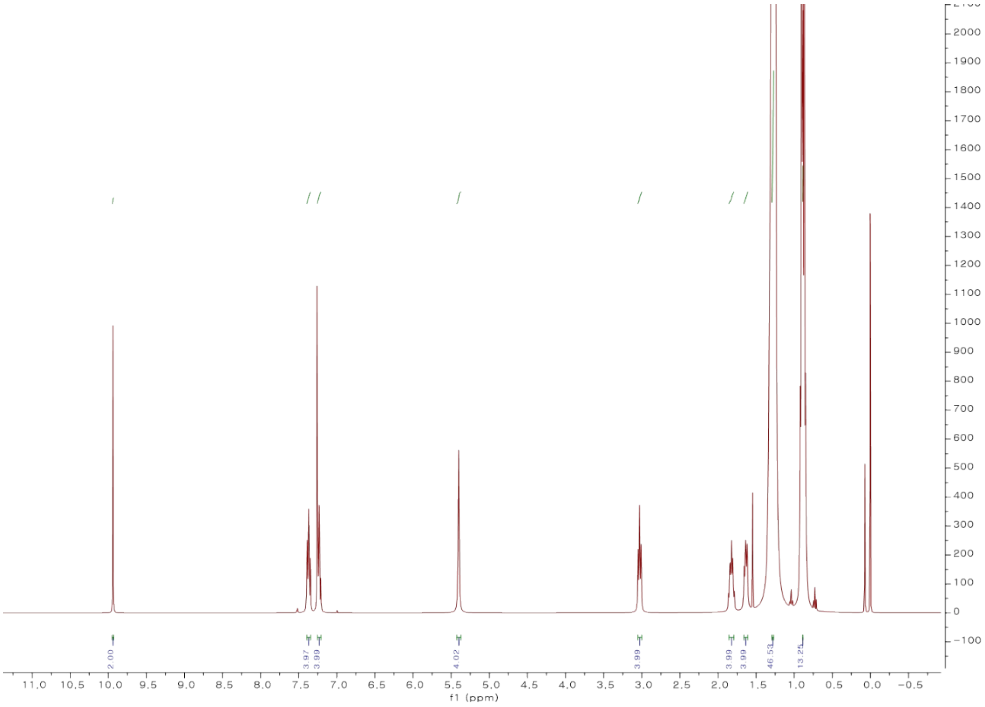

Fig. S25 ^{1}H NMR spectra of compound 4a in $CDCl_3$.

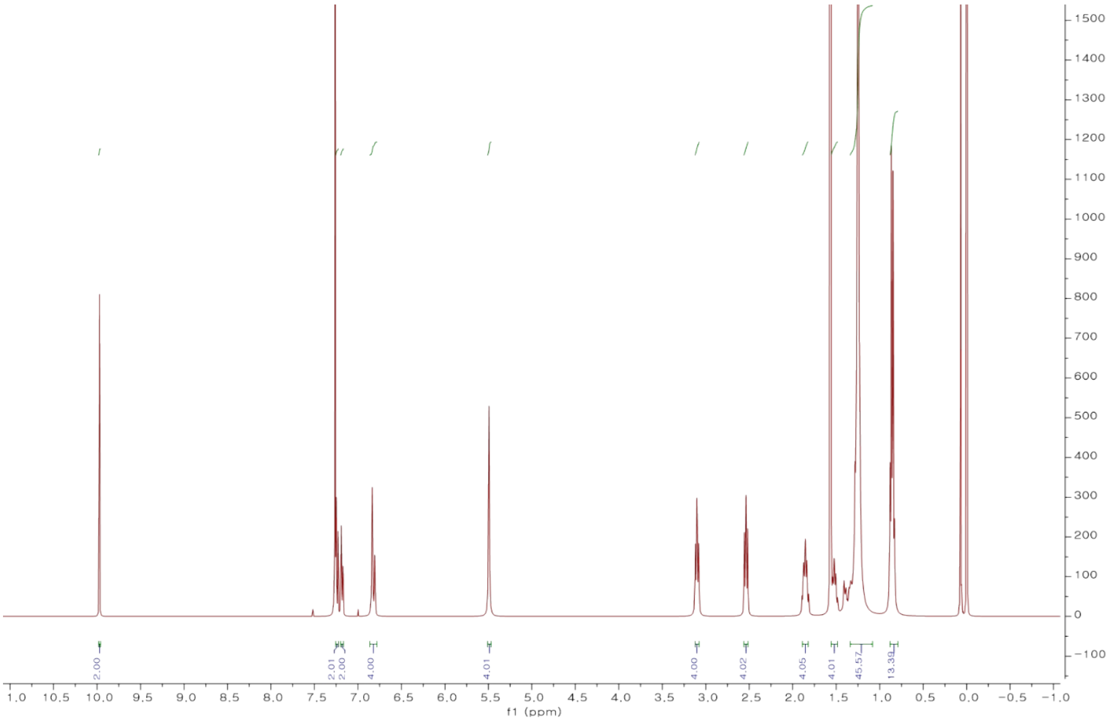

Fig. S26 ^{1}H NMR spectra of compound 4b in $CDCl_3$.

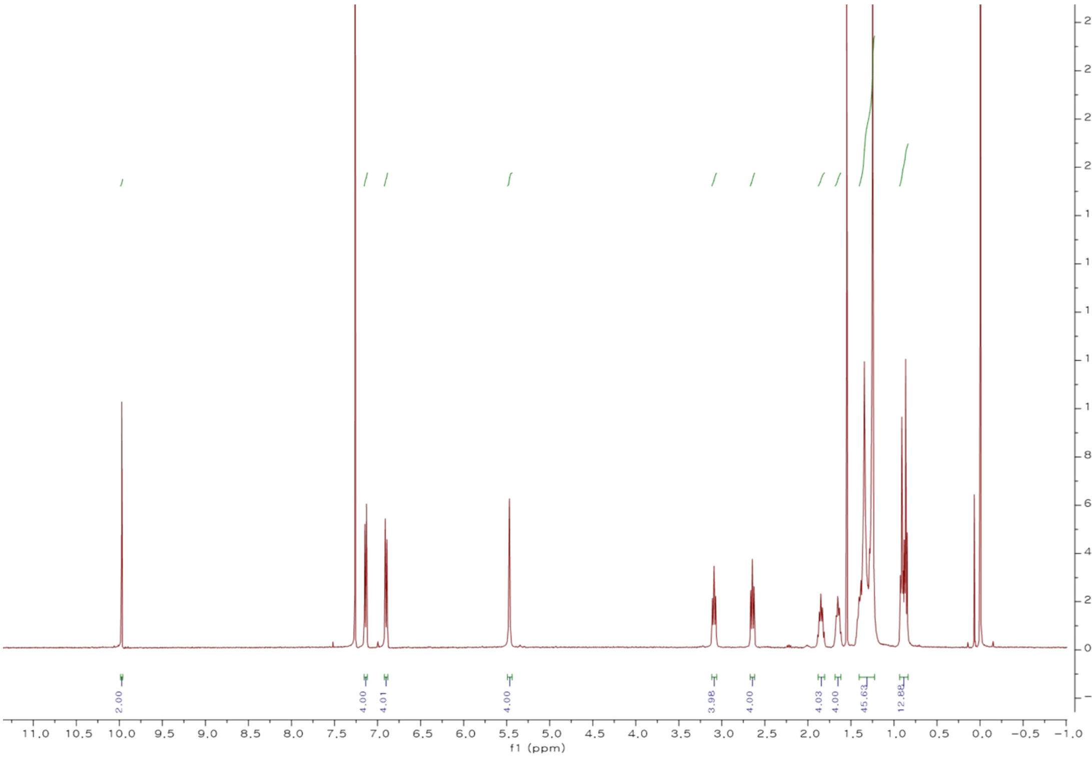

Fig. S27 ^{1}H NMR spectra of compound 4c in $CDCl_3$.

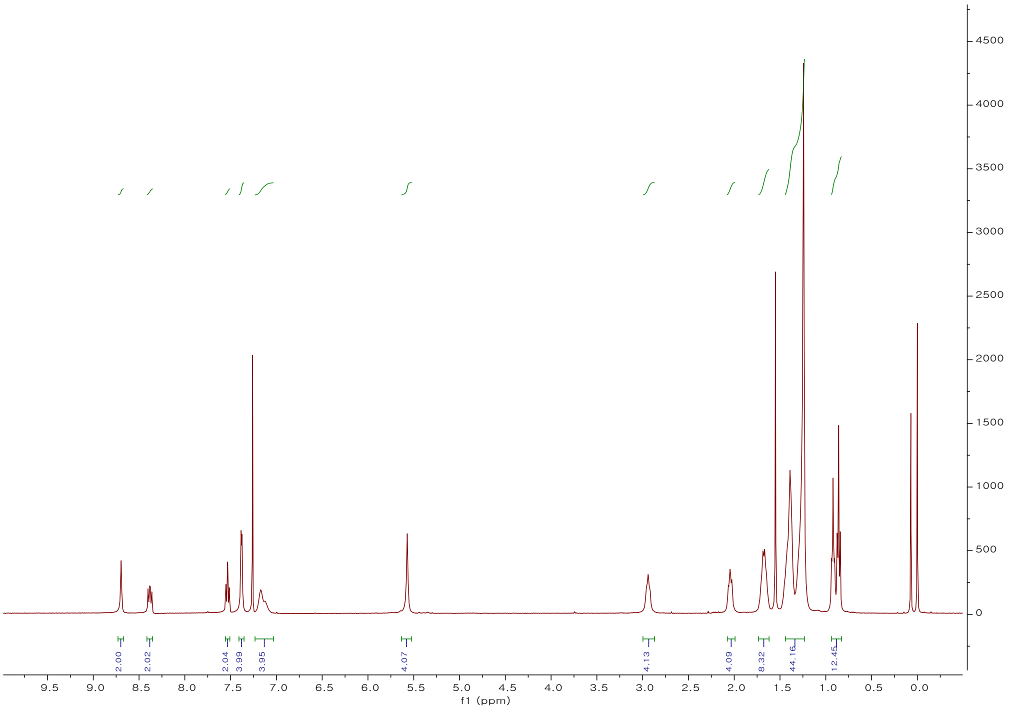

Fig. S28 ^{1}H NMR spectra of *o*-BzY in $CDCl_3$.

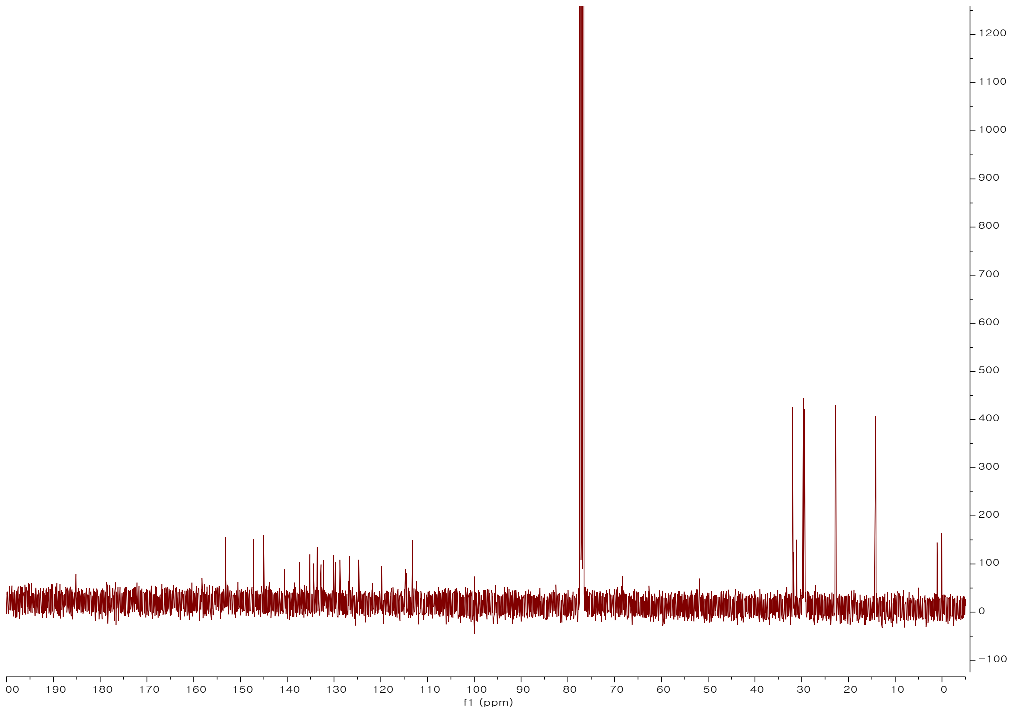

Fig. S29 ^{13}C NMR spectra of *o*-BzY in CDCl$_3$.

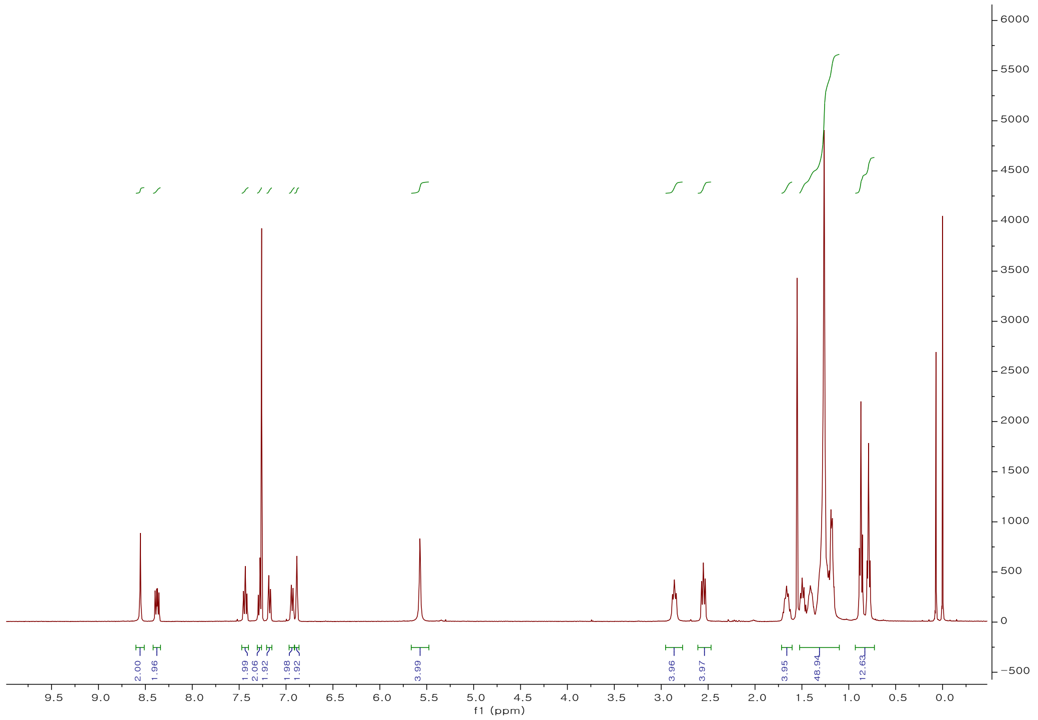

Fig. S30 ^{1}H NMR spectra of *m*-BzY in CDCl$_3$.

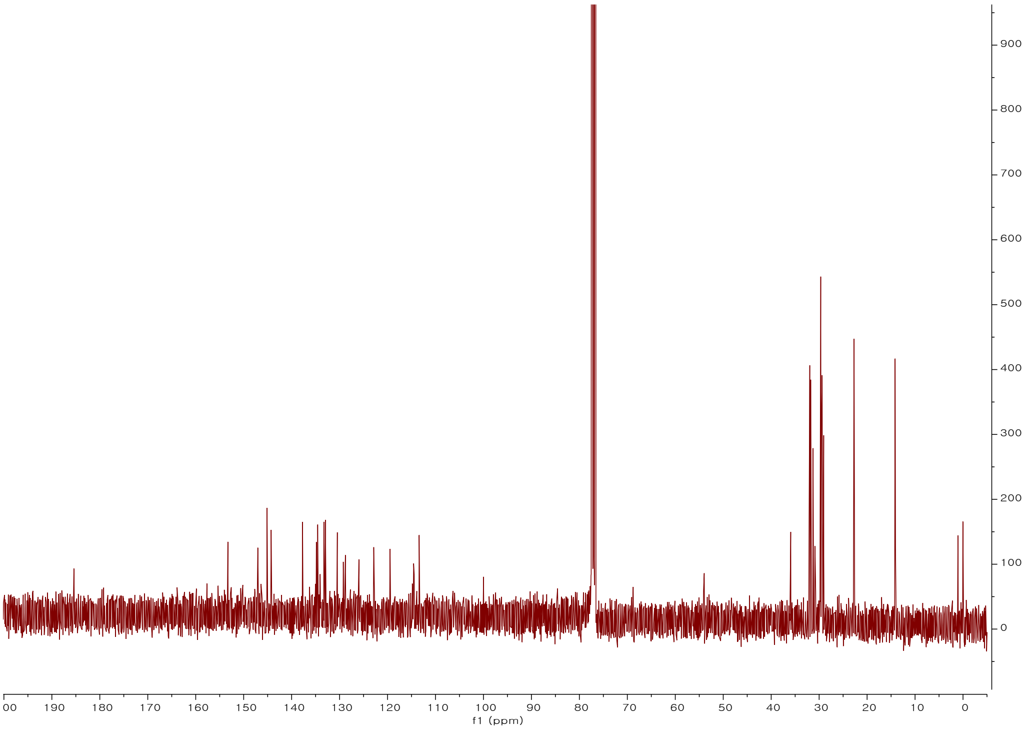

Fig. S31 ^{13}C NMR spectra of *m*-BzY in CDCl$_3$.

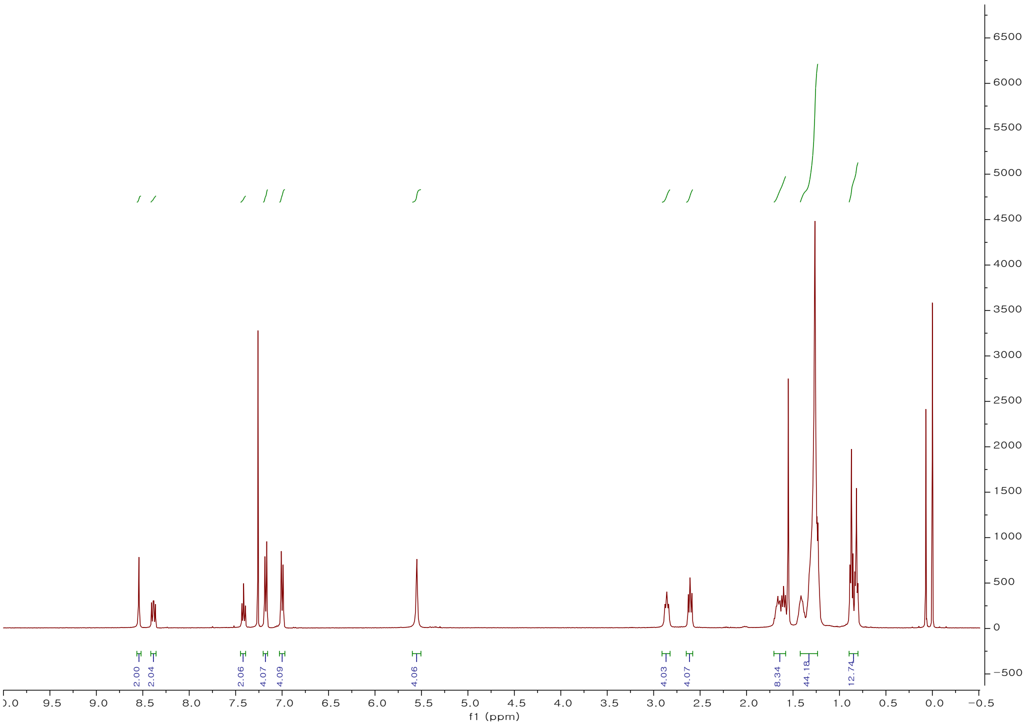

Fig. S32 ^{1}H NMR spectra of *p*-BzY in CDCl$_3$.

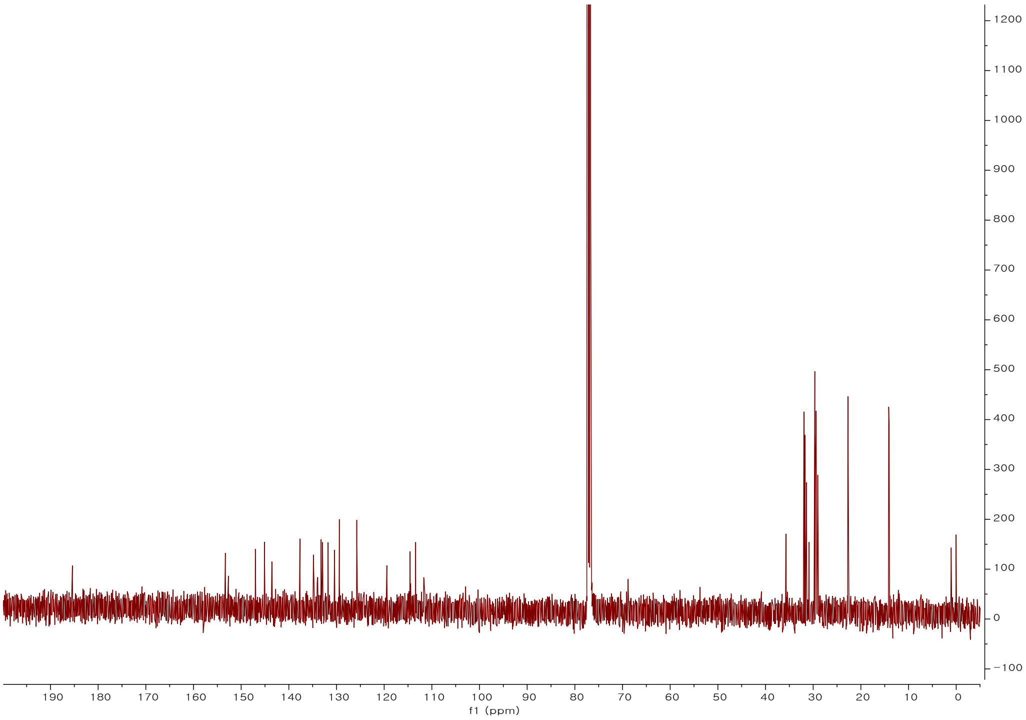

Fig. S33 ^{13}C NMR spectra of *p*-BzY in CDCl$_3$.

References

1 C. Güler, *GIS and Geostatistical Techniques for Groundwater Science*, Elsevier, 2019.

2 W. Su, Q. Fan, X. Guo, J. Wu, M. Zhang and Y. Li, *Phys. Chem. Chem. Phys.*, 2019, **21**, 10660-10666.

3 Q. He, M. Shahid, J. Wu, X. Jiao, F. D. Eisner, T. Hodsden, Z. Fei, T. D. Anthopoulos, C. R. McNeill, J. R. Durrant and M. Heeney, *Adv. Funct. Mater.*, 2019, **29**, 1904956.

4 Y. Liu, M. Li, J. Yang, W. Xue, S. Feng, J. Song, Z. Tang, W. Ma and Z. Bo, *Adv. Energy Mater.*, 2019, **9**, 1901280.

5 K. Wang, X. Song, X. Guo, Y. Wang, X. Lai, F. Meng, M. Du, D. Fan, R. Zhang, G. Li, A. K. K. Kyaw, J. Wang, W. Huang and D. Baran, *Mater. Chem. Front.*, 2020, **4**, 206-212.

6 F. Du, H. Wang, Z. Zhang, L. Yang, J. Cao, J. Yu and W. Tang, *Mater. Horiz.*, 2021, **8**, 1008-1016.

7 Y. Zhao, Y. Liu, X. Liu, X. Kang, L. Yu, S. Dai and M. Sun, *ChemSusChem*, 2021, **14**, 4783-4792.

8 R. Ma, Y. Tao, Y. Chen, T. Liu, Z. Luo, Y. Guo, Y. Xiao, J. Fang, G. Zhang, X. Li, X. Guo, Y. Yi, M. Zhang, X. Lu, Y. Li and H. Yan, *Sci. China Chem.*, 2021, **64**, 581-589.

9 X. Xu, Y. Qi, X. Luo, X. Xia, X. Lu, J. Yuan, Y. Zhou and Y. Zou, *Fundam. res.*, 2022, DOI: https://doi.org/10.1016/j.fmre.2022.01.025.

10 S. He, Z. Lin, F. Du, X. Wang, Y. Liu and W. Tang, *Chem. Eng. J.*, 2022, **441**, 135973.

11 Y. Liu, Z. Lin, J. Cao, F. Du, H. Wang, S. He and W. Tang, *Small*, 2022, **18**, 2201209.

12 D. Li, H. Lu, Y.-N. Chen, X. Ma, H. Zhang, H. Wang, X. Yu, X. Xu, Z. Zhang, X. Xu, Y. Liu, Z. Ma, A. Zhang and Z. Bo, *Chem. Mater.*, 2022, **34**, 8840-8848.